

# **Diffusion studies with X-ray photon correlation spectroscopy**

Diplomarbeit  
zur Erlangung des akademischen Grades  
Magister der Naturwissenschaften  
an der Fakultät für Physik  
der Universität Wien

Eingereicht von Michael Leitner  
Betreut von Ao.Univ.Prof. Bogdan Sepiol

Wien, Februar 2007



## Abstract

Until now, measurements of the elementary diffusion step of atoms in solids by X-ray photon correlation spectroscopy have not been successful due to intensity limitations. The thesis at hand deals with the question of how much scattered intensity is necessary and whether there are samples that yield this scattered intensity. The framework of photon correlation spectroscopy is treated with special attention to the case of low intensities, and a new normalisation rule is proposed. Further theoretical estimates of the signal-to-noise ratio are derived, also an algorithm for simulating a PCS-experiment is given. Using this algorithm, the estimates are confirmed. Also the expected contrast of an XPCS-experiment is calculated, and recipes for optimising the product of contrast and intensity (which turns out to be the relevant quantity for the signal-to-noise ratio) are given. Finally, several samples are considered for measuring the elementary diffusion step, and an experiment on  $\text{Cu}_{90}\text{Au}_{10}$  is proposed.

## Zusammenfassung

Bislang ist es nicht gelungen, den elementaren atomaren Diffusionsschritt in Festkörpern mit Röntgen-Photonenkorrelationsspektroskopie zu messen, da die erforderliche Intensität nicht verfügbar war. Die vorliegende Arbeit beschäftigt sich mit der Frage, wieviel Streuintensität dafür nötig ist und ob es Proben gibt, mit denen diese Intensität erreichbar ist. Dafür wird das theoretische Gebäude der Photonenkorrelationsspektroskopie mit besonderem Augenmerk auf niedrige Intensitäten durchleuchtet und eine neue Normierungsregel wird vorgeschlagen. Weiters werden theoretische Abschätzungen des Verhältnisses von Signal zu Rauschen abgeleitet und ein Algorithmus zur Simulation eines PCS-Experimentes wird vorgelegt. Unter Verwendung dieses Algorithmus werden die Abschätzungen bestätigt. Außerdem wird der erwartete Kontrast eines XPCS-Experimentes berechnet und Anleitungen für die Maximierung des Produkts von Kontrast und Intensität (welches sich als die relevante Größe für das Verhältnis von Signal zu Rauschen herausstellt) gegeben. Schlussendlich werden mehrere mögliche Proben zur Messung des elementaren Diffusionsschrittes betrachtet und ein Experiment mit  $\text{Cu}_{90}\text{Au}_{10}$  vorgeschlagen.

## Acknowledgements

First of all I want to thank the Austrian tax-payer for financing my studies until now and my job in the future. Then I want to thank all the people who personally supported me when writing this thesis. Bogdan Sepiol, my supervisor, always had advice for me, also suggestions about things that otherwise wouldn't have presented themselves to me. Lorenz-Mathias Stadler and Bastian Pfau were the ones I adressed my questions concerning XPCS to, even though they are not in our group any more, they cared for me all the same. Bastian invited me to a stay at BESSY, which was my first (and only, up to now) impression of a synchrotron, and especially Lorenz has devoted many hours of his recent night shifts at the ESRF to proof-reading of this thesis. Manfred Smolik, thank you for sharing my room and allowing me to participate in your work via many discussions about mathematics, my second field of interest, also for bringing some life (i.e. ambrosiae) into my world of dry physics. Without your support in all IT-related problems, life would have been much harder. The last and most enduring thought goes to Alice, together we will take them on.

# Contents

<b>1</b>	<b>Introduction</b>	<b>1</b>
<b>2</b>	<b>Theory of photon correlation spectroscopy</b>	<b>5</b>
2.1	The scattered amplitude . . . . .	5
2.2	The auto-correlation function . . . . .	14
2.3	Poisson noise . . . . .	15
2.4	Normalisation . . . . .	17
2.5	Non-ideal contrast . . . . .	19
<b>3</b>	<b>Simulations</b>	<b>21</b>
3.1	Introductory simulations . . . . .	21
3.2	Verifying our estimates . . . . .	23
3.3	Conclusion . . . . .	36
<b>4</b>	<b>Optimising the beamline-setup</b>	<b>39</b>
4.1	Fundamental layout . . . . .	39
4.2	Contrast and intensity . . . . .	40
<b>5</b>	<b>Optimising the sample</b>	<b>45</b>
5.1	Interaction of X-ray photons with matter . . . . .	45
5.2	Comparing samples . . . . .	46
5.3	Proposing an experiment . . . . .	50
5.4	Discussion of an already performed experiment . . . . .	51
<b>6</b>	<b>Conclusion</b>	<b>55</b>
	<b>Bibliography</b>	<b>59</b>
	<b>Curriculum vitae</b>	<b>61</b>

*Contents*

# 1 Introduction

The *structure* of solids is nowadays relatively well explored. Solids can be divided into glass-like matter, on the one hand, and crystalline matter, on the other hand. In 1912, during an era of dramatic changes in physics, Max von Laue used X-ray radiation—which itself was discovered only 17 years earlier—to produce a diffraction pattern of a crystal. This revolutionary experiment proved the ordered nature of crystals on atomic scales (and was at the same time one of the first direct proofs for the existence of atoms). Since then X-ray scattering has been extensively used to study the static properties of solids, in particular of crystals, and the results can be found in every current textbook on solid state physics, e.g. [Ashcroft76]. Still, the method of X-ray scattering is the only one capable of examining rather large areas of solids on atomic scales. In contrast, there exists a variety of microscopy methods that can be used for producing real-space images with high resolution but are usually restricted to probe only a relatively small part of the sample.

*Dynamics* in solids, on the other hand, is an area of great interest which is much less explored than merely static features because it is so much harder to unravel sample properties that vary in time. As one can often see in old photographs, houses (more generally, non-moving objects) are correctly depicted and sometimes even people are standing and looking into the camera. But quite frequently there are also elongated blurs, stemming from people who did not care about the photographer and walked past. Basically, that was an intensity problem: one had to expose the films rather long, which is no problem for static objects, since one can just wait and the photons are going to come in that case. Let us consider the following problem: one has an elevated position over a square and wants to record the movements of the people crossing the square. With a camera with a minimum exposure time of a minute, as it was the case then, that task cannot be accomplished—the people are moving too fast and no information can be extracted from the image. With today's technology it is possible, of course: you just take one picture every half second and you can follow every person crossing the square. Why is it possible? Because one has better lenses and more sensitive films nowadays. Now, think of a company of soldiers parading across the square. If there are enough men marching, we can see it on the picture even if we have an exposure time of one minute. In some sense, this is the point where the technique of *X-ray photon correlation spectroscopy* (XPCS) stands today. Until now one has not been able to follow the movement of single atoms using XPCS. If, on the other hand, precipitates of about  $10^4$  atoms move through the crystal matrix, one can detect them [Stadler03, Pfau06a, Stadler06a]. The current endeavours to improve the technique of XPCS are not toward more sensitive films, in fact this is not possible due to the corpuscular nature of detecting light, the vision rather is to increase the

## 1 Introduction

illumination of the square, metaphorically speaking, by making use of new light sources. In 2009 the first X-ray free electron laser should become operational, which will yield an “illumination” (more scientifically, the peak brilliance) about  $10^{10}$  times greater than now at disposal [XFEL].

The main goal of the thesis at hand is to decide whether it will be possible to obtain information about diffusion on atomic scales from XPCS measurements. Ideally, the elementary diffusion step, i.e. atomic jump vector and probability, should be resolved by taking full advantage of the predicted XFEL brilliance. Moreover, an assessment is made whether there are some very carefully selected samples that could make possible such measurements even with the brilliance achievable at today’s best light sources, so-called third-generation synchrotrons.

For the sake of completeness one may not omit that diffusion on atomic scales has already been measured, however not with XPCS. In our analogy with the people crossing the place this would be like attaching threads to some of the people and then measuring how fast the threads move. Physically the methods are known as quasi-elastic neutron scattering [Kaisermayr01a], quasi-elastic Mößbauer spectroscopy [Sepiol93], nuclear resonant scattering [Sepiol96] and the neutron-spin echo technique [Kaisermayr01b]. All these methods share the disadvantage that only certain isotopes can be measured. In Mößbauer spectroscopy, for example, the most common isotope by far is  $^{57}\text{Fe}$ , which is the reason why alloys containing iron are intensively investigated. Mapping this to our picture, only some people (really a minority) let you tie threads to them. Another disadvantage of the above methods is their limited energy resolution which makes only very fast diffusion detectable (if you tied the line to a snail, you would need a micrometer-scale to observe the movement).

Enough of snails, back to physics: X-ray photon correlation spectroscopy makes use of a (partially) coherent X-ray beam. If you do not know what that means, [Als-Nielsen01] gives a short introduction, for now: the more laser-like, the more coherent; what we need for the thesis at hand is given in chapter 4. X-ray beams with a relatively high coherent fraction can be obtained at state-of-the-art synchrotrons, where sufficiently small pinholes are used to select only the coherent beam cross-section. Into this beam one puts the sample, where the scattering takes place (the necessary theory of which will be given in chapter 5). Preferably, the scattered photons are recorded with a two-dimensional detector, which is placed at a certain angle to match both the length scales one wants to study (see the hatched detector in Figure 4.1, for example) and counts per pixel and image (“frame”). The coherence effect one uses is well-known from lasers: if one points a laser at a rough surface, one observes so called speckles, i.e. regions in the illuminated spot that look bright and regions which are totally dark. This is an interference effect, depending on the coherence of the light source, which will be mathematically treated in chapter 2. So, if the beam is coherent enough and the size of the pixels of the detector is not too big, one expects to see a speckle pattern in the frame. Since, as it will turn out, the speckle pattern is directly related to the positions of the sample inhomogeneities (be it solute atoms in an otherwise pure crystal, be it vacancies or even whole precipitates), one expects temporally changing speckle patterns, due to the position changes of the inhomogeneities. The quantity one wants to determine for



characterising the dynamics is the correlation time, which will be defined and dealt with in chapter 2. Roughly speaking, the correlation time is the time after which the speckle pattern has lost most of its previous shape and has evolved to something new. The classical way to do this is to compute the auto-correlation function. In case of simple diffusion, this function follows an exponential decay that can be fitted, which directly yields the correlation time, see chapter 2. Recently, a new method was proposed and also successfully applied for analysing the temporally fluctuating speckle intensities, called fluctuation analysis (FA) and its extension detrended fluctuation analysis (DFA), respectively [Stadler06b, Pfau06b]. The DFA-approach is particularly suited for dealing with so-called long-term correlations that decay  $\propto t^{-\gamma}$  with  $0 < \gamma < 1$  [Kandelhardt01]. However, since single-atom diffusion is usually not long-term correlated, for the problem at hand the traditional auto-correlation technique should not be inferior. Furthermore, it is simpler and so allows easier error estimates, which will be a main point of this thesis. In either case, the measurement yields just a few points in  $q$ -space for some temperatures, so one has to decide on a probable model beforehand (based on analogies from results from resonant measurements mentioned above), optimise the experimental setup to be able to record the expected features and then compare the results to the theory and decide whether they match or another model has to be considered.

So, here is the plan: First, we are going to develop the theoretical background needed, i.e. the relations between the processes on atomic scales—with the sample in *equilibrium*—and the observed photon counts via the auto-correlation function. Second, we will give estimates on the uncertainty of the measured auto-correlation function compared to its expected value. Then we will validate these estimates and arrive at a minimal number of photon counts. This will hold quite generally, i.e. for all (X)PCS experiments where photon count is the limiting factor. Third, we will think about the optimum beamline settings for an XPCS experiment. Finally, the properties of several possible samples will be investigated with respect to the feasibility of measuring diffusion at atomic scale.

## *1 Introduction*

## 2 Theory of photon correlation spectroscopy

In this chapter we will start with an atomistic description of the dynamics in a sample and build up our theory of auto-correlation functions and their relationship to the dynamics. The aim is to arrive at an estimate of the uncertainty of the measured auto-correlation function. Along the way several independent results for different special cases will be derived, which will be verified in the next chapter via simulations.

Picture a crystal with fixed orientation and location, formed of  $L$  atoms arranged in a Bravais lattice with the lattice points denominated  $R_j$ . Let the crystal be perfect apart from  $N$  impurities occupying lattice sites, the positions of the impurities being  $r_j$ , the impurities can be vacancies or atoms of other elements. Let  $L \gg N \gg 1$ . Let the temperature and the composition of the sample be chosen so that the positions of the impurities are random and not correlated, the sample being in equilibrium. Fix a vector  $\Delta q$  ( $|\Delta q| = 2q_0 \sin(\frac{2\theta}{2})$  with  $2\theta$  the angle between the incident beam and the detector arm). Let the crystal be illuminated with (for now) perfectly coherent X-rays, resulting in a scattered intensity  $I$ . So let's calculate the evolution of  $I$  in time and work out the implications for the auto-correlation-function  $g_2(t)$ , that is its expected value and uncertainty.

### 2.1 The scattered amplitude

If we want to detect light we can only detect photons. For now we will neglect the influence of single photons (i.e. Poisson statistics), that is the following quantities are the so-called instantaneous intensity and instantaneous amplitude (intensity before applying quantisation). The influence of Poisson statistics will be dealt with in the following chapters.

The measured intensity is given by (neglecting numerical constants and angular dependence)

$$I(\Delta q, t) = \left| \sum_{j=1}^{N+L} f_j e^{i\Delta q \cdot R_j(t)} \right|^2 = \left| f_1 \sum_{j=1}^{N+L} e^{i\Delta q \cdot R_j(t)} + (f_2 - f_1) \sum_{j=1}^N e^{i\Delta q \cdot r_j(t)} \right|^2. \quad (2.1.1)$$

Unless we choose  $\Delta q$  to be a Bragg direction, the first sum in the above equation vanishes, so we get

$$I(\Delta q, t) = \left| \sum_{j=1}^N e^{i\Delta q \cdot r_j(t)} \right|^2, \quad (2.1.2)$$

## 2 Theory of photon correlation spectroscopy

where we also neglect the factor  $(f_2 - f_1)^2$  from now on. The quantity of interest turns out to be the amplitude, given by

$$A(\Delta q, t) = \sum_{j=1}^N e^{i\Delta q \cdot r_j(t)}, \quad (2.1.3)$$

which is just a complex number for fixed  $t$ . Now we compute the probability distribution of the amplitude: As the impurities are randomly located,  $\Delta q \cdot r_j$  (which we will call from now on  $\varphi_j$ ) have to be uniformly distributed on  $[0, 2\pi)$ , so the expected values of the real and the imaginary part of the amplitude of one single impurity has to be 0. Hence we compute  $\sigma_r^2 = \frac{1}{2\pi} \int_0^{2\pi} d\varphi \cos^2(\varphi) = \frac{1}{2}$  for the variance in the real direction, the same for the variance in the imaginary direction. Due to the central limit theorem the probability distribution of the scattered amplitude of the whole sample is a Gaussian in the complex plane centred at 0 with variance  $\frac{N}{2}$ :

$$P_A(x + iy) = \frac{1}{\pi N} \exp\left(-\frac{x^2 + y^2}{N}\right) \quad (2.1.4)$$

Since the intensity is given by the squared amplitude, we get by first transforming to polar coordinates and plugging in  $I = r^2, dI = 2r dr$

$$\frac{1}{\pi N} e^{-\frac{x^2+y^2}{N}} dx dy = \frac{1}{\pi N} e^{-\frac{r^2}{N}} r dr d\varphi = \frac{1}{2\pi N} e^{-\frac{I}{N}} dI d\varphi = \frac{1}{N} e^{-\frac{I}{N}} dI, \quad (2.1.5)$$

which means that the intensity is exponentially distributed with mean  $N$ .

Now we go the other way around: we fix a given amplitude, i.e. we switch our X-ray beam on and observe a certain intensity, by taking the square root we get the modulus of the amplitude, the phase being irrelevant, so we will assume that the amplitude lies on the positive real axis. In order to be able to compute the expected behaviour of the amplitude later in the experiment, we compute the probability distribution of the single amplitudes, which can no longer be uniformly distributed (for  $A > 0$ ). If we think of the canonical ensemble in statistical physics, the answer is clear (there the energy is fixed, here the amplitude is fixed):

$$P(\varphi_j) = \frac{1}{C} e^{\beta \cos(\varphi_j)} \quad \text{for } 0 \leq \varphi < 2\pi. \quad (2.1.6)$$

In our case  $\beta = 2\frac{A}{N}$  (determined by the condition for the expected value of the amplitude) in the limit of big  $N$ ,  $C$  just for normalisation. For a computation using basic probability theory considerations we remember that  $A$  is chosen to be real, so it is given by  $A = x_a + i \cdot 0$ . Since the probability of an event  $E$  under assumptions  $F$  is given by

the probability of observing  $E \cap F$  divided by the probability of  $F$ , we have

$$\begin{aligned}
 P(\phi_1 \leq \varphi_1 \leq \phi_1 + d\phi \mid x_A \leq \sum_{i=1}^N \cos(\varphi_i) \leq x_a + dx \wedge 0 \leq \sum_{i=1}^N \sin(\varphi_i) \leq 0 + dy) &= \\
 = \frac{\frac{1}{2\pi} d\phi \frac{1}{\pi(N-1)} \exp(-\frac{(x_a - \cos(\varphi_1))^2}{N-1}) dx \exp(-\frac{\sin^2(\varphi_1)}{N-1}) dy}{\frac{1}{\pi N} \exp(-\frac{x_a^2}{N}) dx \exp(-\frac{0}{N}) dy} &= \\
 = \frac{1}{2\pi} d\phi \frac{N}{N-1} \exp(-\frac{x_a^2 - 2x_a \cos(\varphi_1) + 1}{N-1} + \frac{x_a^2}{N}) &= \\
 = \frac{1}{2\pi} \frac{N}{N-1} \exp(-\frac{\frac{x_a^2}{N} + 1}{N-1}) \exp(\frac{2x_a \cos(\varphi_1)}{N-1}). & \quad (2.1.7)
 \end{aligned}$$

This should be a probability density function, that means by integrating over  $\varphi_1$  one should get 1 for all  $x_A$ , which is not the case. Remember, however, that we have used the central limit theorem, which can deviate from the exact value considerably in regions of low probability, i.e. for big  $x_A$ . So we just keep the  $\varphi_1$ -dependency and arrive at the above prediction. Since we want to stay in the limit of big  $N$ , we expand (2.1.7) into a Taylor series in  $2\frac{A}{N} \cos(\varphi_j)$ :

$$P(\varphi_j) = \frac{1}{C} \left( 1 + 2\frac{A}{N} \cos(\varphi_j) + O\left(\frac{A^2}{N^2}\right) \right), \quad (2.1.8)$$

and since  $A$  has expected value 0 and standard deviation  $\sqrt{N}$ , we can neglect the terms of higher order and arrive at

$$P(\varphi_j) = \frac{1}{2\pi} \left( 1 + 2\frac{A}{N} \cos(\varphi_j) \right). \quad (2.1.9)$$

We define

$$d := \int_0^{2\pi} d\varphi P(\varphi) \cos(\varphi) = \frac{A}{N} \quad (2.1.10)$$

and

$$e := \int_0^{2\pi} d\varphi P(\varphi) \cos(2\varphi) = 0. \quad (2.1.11)$$

Now we define the quantities

$$a := \sum_{j=1}^{\varepsilon} p_j \cos(s_j \cdot \Delta q) \quad (2.1.12)$$

and

$$b := \sum_{j=1}^{\varepsilon} p_j \cos(2s_j \cdot \Delta q), \quad (2.1.13)$$

## 2 Theory of photon correlation spectroscopy

where the  $s_j$  are the possible jump vectors and the  $p_j$  the probabilities for the jumps,  $\varepsilon$  is just a bound over which the probability for the jumps are too small. If we take  $\varepsilon$  to be the number of nearest neighbours, all  $s_j$  have equal probability  $\frac{1}{\varepsilon}$ .

Now we are ready to investigate the time evolution of the expected value of the amplitude  $A(t)$ : For computing the number of impurities  $N_j$  jumping exactly  $j$  times during an observation time  $t$ , when the average jump frequency is  $s$ , we state the differential equations  $-\dot{N}_0(t) = N_0(t) \cdot s$  and  $\dot{N}_{j+1}(t) = N_j(t) \cdot s - N_{j+1}(t) \cdot s$  (under the assumption that the single jumps of one impurity are not correlated, this condition will not be fulfilled if the impurities are solute atoms diffusing by vacancies, for a treatment of correlated jumps see the end of this section). These equations are solved by a Poisson distribution :

$$N_j(t) = N \frac{(st)^j}{j!} e^{-st} \quad (2.1.14)$$

We have to keep in mind that this is just the expected value, proceeding with the exact probability distribution, however, would be a modification vanishing for  $N \rightarrow \infty$ . Then we understand that the expected value of the amplitude  $A(t)$  is always a real positive number, once we have made the assumption  $A(0) > 0$ . By denoting the probability density function for the difference in  $\varphi$  after  $j$  jumps with  $s^j(\varphi)$  we can write

$$\begin{aligned} EV(A_j(t)) &= \int_0^{2\pi} d\varphi (P * s^j)(\varphi) \cos \varphi \\ &= \int_0^{2\pi} d\varphi \int_0^{2\pi} d\varphi_1 P(\varphi_1) s^j(\varphi - \varphi_1) \cos(\varphi) \\ &= \int_0^{2\pi} d\varphi_1 P(\varphi_1) \int_0^{2\pi} d\varphi s^j(\varphi - \varphi_1) \cos(\varphi) \\ &= \int_0^{2\pi} d\varphi_1 P(\varphi_1) (s^j * \cos)(\varphi_1), \end{aligned} \quad (2.1.15)$$

for the amplitude resulting from a single impurity jumping  $j$  times.  $s^1(\varphi)$  is given by

$$s^1(\varphi) = \sum_{j=1}^L p_j \delta_{(s_j \cdot \Delta q)}(\varphi) \quad (2.1.16)$$

in the terminology of (2.1.12), in fact (2.1.12) is just the expected value of  $\cos(\varphi)$  for this probability distribution, and each function  $s^j(\varphi)$  is just the convolution of  $j$  functions  $s^1(\varphi)$ .

Using that  $s^1(\varphi)$  is symmetric since we have a Bravais lattice we obtain

$$\begin{aligned} (s^1 * \cos)(\varphi) &= \int_0^{2\pi} d\varphi_1 s^1(\varphi_1) \cos(\varphi - \varphi_1) = \text{Re}(e^{i\varphi} \int_0^{2\pi} d\varphi_1 s^1(\varphi_1) e^{-i\varphi_1}) = \\ &= \cos(\varphi) \int_0^{2\pi} d\varphi_1 s^1(\varphi_1) \cos(\varphi_1) = a \cos(\varphi) \end{aligned} \quad (2.1.17)$$

and so

$$\begin{aligned} s^n * \cos &= (s^{n-1} * s^1) * \cos = s^{n-1} * (s^1 * \cos) = a(s^{n-1} * \cos) = \dots \\ &= a^n \cos. \end{aligned} \quad (2.1.18)$$

Similarly

$$s^n * \cos(2.) = b^n \cos(2.). \quad (2.1.19)$$

With these calculations (2.1.15) simplifies to

$$EV(A_j(t)) = a^j \int_0^{2\pi} d\varphi_1 P_A(\varphi_1) \cos(\varphi_1), \quad (2.1.20)$$

if we plug in our simplification (2.1.9), it becomes

$$EV(A_j(t)) = \frac{A(0)}{N} N_j a^j. \quad (2.1.21)$$

As the expected value is linear, we can readily compute

$$\begin{aligned} EV(A(t)) &= \sum_{j=0}^{\infty} N_j EV(A_j(t)) = \sum_{j=0}^{\infty} N \frac{(st)^j}{j!} e^{-st} \frac{A(0)}{N} a^j \\ &= A(0) \sum_{j=0}^{\infty} \frac{(ast)^j}{j!} e^{-st} = A(0) e^{-st} e^{ast} \sum_{j=0}^{\infty} \frac{(ast)^j}{j!} e^{-ast} \\ &= A(0) e^{(a-1)st}. \end{aligned} \quad (2.1.22)$$

Let us dwell on this fact a little: We have connected the behaviour of the amplitude at a given  $\Delta q$ -value (until now just the expected value) with the time passed  $t$ , the jump rate of the impurities  $s$ , which is a function of the temperature for a fixed sample, and a quantity  $a$ , which is a measure of how much the amplitude of one single impurity changes in the mean in one jump. Moreover, the relationship fulfills our expectation of relaxations of fluctuations, that is the expected value decreases exponentially. So now we are going to compute the standard deviation, which gives us by the central limit theorem all the information about the behaviour of the amplitude.

Our first step is to calculate the standard deviation of the change in the real part of the amplitude of one impurity that performs  $j$  jumps, for the sake of clearness we drop

## 2 Theory of photon correlation spectroscopy

the integration boundaries:

$$\begin{aligned}
\sigma_r^2 &= \int P(\varphi) d\varphi \int d\varphi_1 s^j(\varphi_1) (\cos(\varphi - \varphi_1) - \cos(\varphi))^2 - \\
&\quad - \left( \int P(\varphi) d\varphi \int d\varphi_1 s^j(\varphi_1) \cos(\varphi - \varphi_1) - \cos(\varphi) \right)^2 \\
&= \int P(\varphi) d\varphi \int d\varphi_1 s^j(\varphi_1) \left( \frac{1}{2} + \frac{1}{2} \cos(2\varphi - 2\varphi_1) - 2 \cos(\varphi - \varphi_1) \cos(\varphi) + \cos^2(\varphi) \right) \\
&\quad - \left( \int d\varphi P(\varphi) ((s^j * \cos)(\varphi) - \cos(\varphi)) \right)^2 \\
&= \int d\varphi P(\varphi) \left( \frac{1}{2} + \frac{1}{2} \cos(2\varphi) b^j - 2 \cos^2(\varphi) a^j + \cos^2(\varphi) \right) \\
&\quad - (a^j - 1)^2 \left( \int d\varphi P(\varphi) \cos(\varphi) \right)^2 \\
&= \int d\varphi P(\varphi) \left( 1 + \frac{1}{2} \cos(2\varphi) b^j - a^j (1 + \cos(2\varphi)) + \frac{1}{2} \cos(2\varphi) \right) - (a^j - 1)^2 d^2 \\
&= 1 + \frac{1}{2} b^j e - a^j (1 + e) + \frac{1}{2} e - (a^j - 1)^2 d^2, \tag{2.1.23}
\end{aligned}$$

in the limit of  $N \rightarrow \infty$

$$\sigma_r^2 = 1 - a^j, \tag{2.1.24}$$

in this limit the standard deviation of the imaginary part is the same:

$$\sigma_i^2 = 1 - a^j, \tag{2.1.25}$$

because the differences are of order  $e$  and  $d^2$ , which we will neglect in the course of this thesis.

As we want to compute the standard deviation of the amplitude of the whole sample, i.e. the sum over the amplitudes of the single impurities, we have to mind the covariances. One would think that they are zero, at least in the limit  $N \rightarrow \infty$ , but it turns out that they are in fact responsible for the behaviour of the sum. The reason is that we have only a finite number of impurities, and once one impurity has jumped, the probability distribution on the unitary circle in the complex plane has to be modified. Mathematically speaking we need the probability distribution  $P(\varphi_1, \varphi_2)$ . Let us first look into the discrete case, where we do not have a probability distribution on the interval  $[0, 2\pi) \times [0, 2\pi)$ , but rather values  $p_{ij}$  for  $1 \leq i, j \leq M$  with  $\sum_{i=1}^M \sum_{j=1}^M p_{ij} = 1$ . We have  $N$  numbered balls arbitrarily thrown into  $M$  jars, by throwing dice we select one ball and look to which jar it belongs, this gives probability values  $p_j$  for the selected ball being in jar  $j$ . The question is: What are the values  $p_{jk}$  for selecting two balls, the first being in jar  $j$  and the second in jar  $k$ ? By determining the first ball and taking it out, we diminish the number of balls by one to  $N - 1$ , the number of balls in each jar stays the same except in jar  $j$ , where it is one less. So  $p_{jk}$  is given



## 2.1 The scattered amplitude

by  $p_{jk} = p_j(p_k \frac{N}{N-1} - \delta_{j,k} \frac{1}{N-1})$ . Having mastered the discrete case, we generalise to the continuous case, where the two-phase-probability distribution is given by

$$P(\varphi_1, \varphi_2) = P(\varphi_1) \left( P(\varphi_2) \frac{N}{N-1} - \delta(\varphi_1, \varphi_2) \frac{1}{N-1} \right). \quad (2.1.26)$$

So let us compute the covariance (one impurity jumps  $i$  times, the other  $j$  times):

$$\begin{aligned} C_{i,j} &= \int d\varphi_1 d\varphi_2 P(\varphi_1, \varphi_2) \times \\ &\quad \int d\varphi_3 s^i(\varphi_3) (\cos(\varphi_1 - \varphi_3) - \cos(\varphi_1)) \int d\varphi_4 s^j(\varphi_4) (\cos(\varphi_2 - \varphi_4) - \cos(\varphi_2)) - \\ &\quad \left( \int P(\varphi) d\varphi \int d\varphi_1 s^i(\varphi_1) \cos(\varphi - \varphi_1) - \cos(\varphi) \right) \times \\ &\quad \left( \int P(\varphi) d\varphi \int d\varphi_1 s^j(\varphi_1) \cos(\varphi - \varphi_1) - \cos(\varphi) \right) \\ &= \int d\varphi_1 d\varphi_2 P(\varphi_1, \varphi_2) (\cos(\varphi_1) a^i - \cos(\varphi_1)) (\cos(\varphi_2) a^j - \cos(\varphi_2)) - \\ &\quad -(a^i - 1)(a^j - 1) d^2 \\ &= \frac{N}{N-1} \int d\varphi_1 d\varphi_2 P(\varphi_1) P(\varphi_2) \cos(\varphi_1) \cos(\varphi_2) (a^i - 1)(a^j - 1) \\ &\quad - \frac{1}{N-1} \int d\varphi_1 d\varphi_2 P(\varphi_1) \delta(\varphi_1, \varphi_2) \cos(\varphi_1) \cos(\varphi_2) (a^i - 1)(a^j - 1) - \\ &\quad (a^i - 1)(a^j - 1) d^2 \\ &= \frac{N}{N-1} (a^i - 1)(a^j - 1) d^2 - \frac{1}{N-1} \frac{1}{2} (a^i - 1)(a^j - 1) - (a^i - 1)(a^j - 1) d^2 \\ &= (a^i - 1)(a^j - 1) \left( d^2 \frac{1}{N-1} - \frac{1}{2} \frac{1}{N-1} \right), \end{aligned} \quad (2.1.27)$$

in the limit  $N \rightarrow \infty$

$$C_{i,j} = -(a^i - 1)(a^j - 1) \frac{1}{2} \frac{1}{N-1}. \quad (2.1.28)$$

## 2 Theory of photon correlation spectroscopy

By  $V(\sum_i X_i) = \sum_i V(X_i) + 2 \sum_{i < j} C(X_i, X_j)$  we arrive at (in the above limit)

$$\begin{aligned}
\sigma_r^2 &= \sum_{i=1}^{\infty} N_i(t)(1 - a^i) - \\
&\quad - \frac{1}{2(N-1)} \left( \sum_{i=1}^{\infty} \sum_{j=1}^{\infty} N_i(t)N_j(t)(a^i - 1)(a^j - 1) - \sum_{i=1}^{\infty} N_i(t)(a^i - 1)^2 \right) \\
&= N(1 - e^{(a-1)st}) - \frac{1}{2(N-1)} \left( N^2(1 - e^{(a-1)st})^2 - \sum_{i=1}^{\infty} N_i(t)(a^{2i} - 2a^i + 1) \right) \\
&= N \left( 1 - e^{(a-1)st} - \right. \\
&\quad \left. - \frac{1}{2(N-1)} (N(1 - 2e^{(a-1)st} + e^{2(a-1)st}) - e^{(a^2-1)st} + 2e^{(a-1)st} - 1) \right) \\
&\approx N(1 - e^{(a-1)st} - \frac{1}{2} + e^{(a-1)st} - \frac{1}{2}e^{2(a-1)st}) = \frac{N}{2}(1 - e^{2(a-1)st}), \quad (2.1.29)
\end{aligned}$$

the same holds for  $\sigma_i^2$ . This is not surprising if we consider two special cases: Firstly, the limit of  $t \rightarrow \infty$ ,  $\sigma^2$  tends to  $\frac{N}{2}$  in this case, which is the well known fact (2.1.4). Secondly, the limit of small  $t$ , here we have  $\sigma^2 = N(1 - a)st$ . Now a short excursion into pure mathematics: let  $f(x, y)$  be a centred Gaussian in  $\mathbb{R}^2$  with some fixed  $\sigma$ :

$$f(x, y) = \frac{1}{2\pi\sigma^2} \exp\left(-\frac{x^2 + y^2}{2\sigma^2}\right), \quad (2.1.30)$$

$u(x, y, t)$  too, but with a time-dependent standard deviation  $\sigma_t$ :

$$u(x, y, t) = \frac{1}{2\pi\sigma_t^2} \exp\left(-\frac{x^2 + y^2}{2\sigma_t^2}\right). \quad (2.1.31)$$

Now we define a contraction

$$F_t(f(\cdot)) := d_t^2 f(\cdot \cdot d_t) \quad (2.1.32)$$

and we compute the necessary condition for our coefficients for the following equation to be fulfilled:

$$F_t(f * u(\cdot, t)) = f \quad (2.1.33)$$

Plugging in gives

$$\frac{d_t^2}{2\pi(\sigma_t^2 + \sigma^2)} \exp\left(-\frac{x^2 + y^2}{2} \frac{d_t^2}{\sigma^2 + \sigma_t^2}\right) = \frac{1}{2\pi\sigma^2} \exp\left(-\frac{x^2 + y^2}{2\sigma^2}\right), \quad (2.1.34)$$

so our condition is  $\sigma^2 + \sigma_t^2 = \sigma^2 d_t^2$ . Now let us fill our abstract calculations with life (i.e. physics): the probability distribution of the amplitude (without other information) is by (2.1.4) a Gaussian with variance  $\frac{N}{2}$ . Now we fix a point (i.e. an amplitude) in

the complex plane. Waiting a short time  $t$ , the expected value of the amplitude moves towards 0 due to (2.1.22), and because  $t$  is small, the distribution of the amplitude is a Gaussian around the expected value due to the central limit theorem. So the initial distribution gets more peaked on the one hand because of the relaxation of the fluctuations, on the other hand new fluctuations arise. Because we are in equilibrium, the distribution of the amplitudes has to be independent of time, so the two effects have to cancel each other. That is what we have computed above. We know that  $d_t = e^{(a-1)st}$  from (2.1.22), therefore we need  $\sigma_t^2 = \sigma^2(d_t^2 - 1) = \frac{N}{2}(1 - 2(a-1)st - 1) = N(1-a)st$  in the limit of small  $t$ , exactly as we have seen above.

To sum up, we have the probability distribution for the amplitude of  $N$  scatterers at time  $t$ , when the amplitude at time  $t = 0$  was given by  $A(0) > 0$ :

$$P_{A(t)}(x + iy) = \frac{1}{\pi N(1 - e^{2(a-1)st})} \exp\left(-\frac{(x - A(0)e^{(a-1)st})^2 + y^2}{N(1 - e^{2(a-1)st})}\right) \quad (2.1.35)$$

### Correlated jumps

In a pure monoatomic crystal, i.e. the only impurities are (very few) vacancies, the jumps of the vacancies are not correlated, because due to the very low concentration, in the vicinity of a vacancy all other lattice site will be occupied, so there are no preferred directions, and if it jumps, the new situation is exactly like the old one. For interstitial diffusers with very few solute atoms this holds too, because equivalent interstitial sites in a Bravais lattice form again a Bravais lattice. This is not the case when we consider diffusion of a solute by vacancies. The solute atom needs a vacancy to jump, in fact it swaps place with the vacancy, so the moment it has jumped (say) to the right, it has on its left side a vacancy and the probability that it jumps right away back is much higher than for a jump in another direction. When we consider the case that there are far more solute atoms than vacancies (which will generally be the case, since a typical number of vacancies per matrix atom is  $10^{-7}$  at low temperatures, near the melting temperature about  $10^{-4}$ ), then we see that only successive jumps of solute atoms are correlated, since there is only one vacancy around and its position is determined by the last jump. Then one can treat the problem by the so-called encounter model, for example treated in [Vogl98]: Picture a solute atom and its vicinity, which is free of other solutes or vacancies. Then a vacancy enters the vicinity, it will probably exchange place with the solute atom a few times and then leave the vicinity again. Since the frequency of vacancies entering the vicinity is far lower than the jump frequency of the solute atom once a vacancy is present, the process has two time scales, and if one measures at time scales in the range of vacancies entering the vicinity, the fast jumps of the solute atom with vacancy present can be treated as one jump. So the formalism above holds, one has to compute the probabilities of the many jumps treated as one, which will give non-zero probabilities for non-nearest-neighbour jumps. One has also to keep in mind that the quantity  $s$  now is the frequency of vacancies entering the vicinity of the solute atom.

## 2.2 The auto-correlation function

In an (X-ray) photon correlation spectroscopy experiment one measures the intensity at a number of points in  $q$ -space over the duration of the experiment. We single out one such point and look at the intensity as a function of time:  $I = I(t)$ . In particular if we think about measuring intensity time series using a CCD camera, we have to account for the finite exposure (and readout) time of each picture (“frame”), so  $I = I_k, 1 \leq k \leq K$ , if we divide the experiment duration into  $K$  timesteps. One method for evaluating the experimental data of samples in equilibrium is by calculating the intensity auto-correlation function for each (recorded) point in  $q$ -space:

$$g_2(t) = \frac{1}{C} \int dt' I(t') I(t' + t) \quad (2.2.1)$$

or rather

$$g_2(\Delta k) = \frac{1}{C} \frac{K}{K - \Delta k} \sum_{k=1}^{K-\Delta k} I_k I_{k+\Delta k}, \quad (2.2.2)$$

where the normalisation factor  $C$  is determined so that  $\lim_{t \rightarrow \infty} g_2(t) = 1$ .  $C$  is dealt with later, for now we will just assume that  $g_2(t)$  decays to 1. We will also neglect the influence of the finite exposure times and Poisson noise.

Now we define

$$\begin{aligned} F(x_1, \sigma) &:= \int dx dy (x^2 + y^2) \frac{1}{2\pi\sigma} e^{-\frac{(x-x_1)^2+y^2}{2\sigma^2}} \\ &= \int dx dy ((x+x_1)^2 + y^2) \frac{1}{2\pi\sigma} e^{-\frac{x^2+y^2}{2\sigma^2}} \\ &= \frac{1}{\pi} \int dx dy ((\sqrt{2}\sigma x + x_1)^2 + (\sqrt{2}\sigma y)^2) e^{-x^2-y^2} \end{aligned} \quad (2.2.3)$$

For expanding into a Taylor series in  $\sigma$  we compute the derivatives:

$$\frac{d}{d\sigma} F(x_1, \sigma) = \frac{1}{\pi} \int dx dy (2\sqrt{2}(\sqrt{2}\sigma x + x_1)x + 4\sigma y^2) e^{-x^2-y^2}$$

$$\frac{d^2}{d\sigma^2} F(x_1, \sigma) = \frac{1}{\pi} \int dx dy (4x^2 + 4y^2) e^{-x^2-y^2}$$

$$\frac{d^3}{d\sigma^3} F(x_1, \sigma) = 0$$

$$F(x_1, 0) = x_1^2$$

$$\frac{d}{d\sigma} F(x_1, 0) = 0$$

$$\frac{d^2}{d\sigma^2} F(x_1, 0) = 4 \frac{1}{\pi} 2\pi \int r dr r^2 e^{-r^2} = 8 \int_0^\infty r dr e^{-r^2} = 4$$

so  $F(x, \sigma)$  is given by

$$F(x, \sigma) = x^2 + 2\sigma^2 \quad (2.2.4)$$

So we have for the expected value of the autocorrelation function  $g_2$  for shift time  $t$

$$\begin{aligned} E(g_2(t)) &\propto \int_0^\infty dI \frac{I}{N} e^{-\frac{I}{N}} F\left(\sqrt{I} e^{(a-1)st}, \sqrt{\frac{N}{2}(1 - e^{2(a-1)st})}\right) \\ &= \int_0^\infty dI \frac{I}{N} e^{-\frac{I}{N}} \left( I e^{2(a-1)st} + N(1 - e^{2(a-1)st}) \right) \\ &= N^2(1 - e^{2(a-1)st}) + e^{2(a-1)st} 2N^2 \\ &= N^2(1 + e^{2(a-1)st}). \end{aligned} \quad (2.2.5)$$

Without taking into account Poisson noise, boundary effects, finite exposure times or non-ideal coherence, we see that the normalisation factor under these circumstances is given by  $N^2$ , which is by (2.1.5) just the squared mean intensity. We further see that the auto-correlation function has exponential form with offset 1, and we have connected the coefficient in the exponent with the processes on atomic level.

## 2.3 Poisson noise

Until now we have not taken into account the quantisation of the radiation. For the expected value of the auto-correlation function we have only needed the expected value of the intensity, which is unaffected by the quantisation. Now we are going to have a first look into the predicted standard deviation of the measured auto-correlation function, which is dominated by the expected number of photons per frame  $\bar{I}$  (we assume constant beam intensity):

In order to get an analytic result, unfortunately without great significance, we compute the variance of the auto-correlation function of a data set  $I_k$ ,  $1 \leq k \leq K$ , where the frame exposure times are short compared to the correlation time and the intervals between two frames much longer than the correlation time which means that the instantaneous intensities at the time steps  $k$  are not correlated. Now we have to keep in mind two instances: Firstly, the instantaneous intensity, which is by (2.1.5) exponentially distributed,  $P(I) = \frac{1}{I} e^{-\frac{I}{I}}$ , secondly, the actual number of photons per frame with fixed instantaneous intensity, which has a Poisson distribution with parameter  $I$ :  $P(n) = \frac{I^n}{n!} e^{-I}$  [Goodman85]. The Poisson distribution with parameter  $I$  has expected value  $I$  and variance  $I$ . So the actual probability of detecting  $n$  photons is  $\int_0^\infty dI \frac{1}{I} e^{-\frac{I}{I}} \frac{I^n}{n!} e^{-I}$ . By

$$\int_0^\infty dI \frac{1}{I} e^{-\frac{I}{I}} \sum_{n=0}^\infty \frac{I^n}{n!} e^{-I} n = \int_0^\infty dI \frac{1}{I} e^{-\frac{I}{I}} I = \bar{I} \quad (2.3.1)$$

and

$$\int_0^\infty dI \frac{1}{I} e^{-\frac{I}{I}} \sum_{n=0}^\infty \frac{I^n}{n!} e^{-I} n^2 = \int_0^\infty dI \frac{1}{I} e^{-\frac{I}{I}} (I + I^2) = \bar{I} + 2\bar{I}^2, \quad (2.3.2)$$

## 2 Theory of photon correlation spectroscopy

where we have made use of the fact that the second moment is the sum of expected value and variance, we can compute the covariance of two points of the not normalised auto-correlation function with neglected boundary effects (for every point we average over  $K$  correlated pairs, if  $k + \Delta k > K$ , we take  $k + \Delta k - K$ ) - the expected value is given by  $\bar{I}^2$ :

$$\begin{aligned} C_{\Delta k, \Delta l} &= EV \left( \left( \frac{1}{K} \sum_{k=1}^K I_k I_{k+\Delta k} - \bar{I}^2 \right) \left( \frac{1}{K} \sum_{l=1}^K I_l I_{l+\Delta l} - \bar{I}^2 \right) \right) \\ &= EV \left( \frac{1}{K^2} \sum_{k=1}^K I_k I_{k+\Delta k} \sum_{l=1}^K I_l I_{l+\Delta l} \right) - \bar{I}^4 \end{aligned} \quad (2.3.3)$$

If  $\Delta k \neq \Delta l$ , we have  $4K$  terms in the double sum where one timestep appears in the left product and simultaneously in the right, so we get

$$C_{\Delta k, \Delta l} = \frac{1}{K} ((K^2 - 4K)\bar{I}^4 + 4K\bar{I}^2(\bar{I} + 2\bar{I}^2)) - \bar{I}^4 = \frac{4}{K}(\bar{I}^3 + \bar{I}^4). \quad (2.3.4)$$

If  $\Delta k = \Delta l$ , we are calculating in fact the variance and we have  $2K$  terms where one timestep appears in the left and in the right product, and we have  $K$  terms where both timesteps appear on the left and on the right, so:

$$\begin{aligned} V_{\Delta k} &= \frac{1}{K} ((K^2 - 3K)\bar{I}^4 + 2K\bar{I}^2(\bar{I} + 2\bar{I}^2) + K(\bar{I} + 2\bar{I}^2)(\bar{I} + 2\bar{I}^2)) - \bar{I}^4 = \\ &= \frac{1}{K}(\bar{I}^2 + 6\bar{I}^3 + 5\bar{I}^4). \end{aligned} \quad (2.3.5)$$

For a first rough estimate we remember that the correct normalisation is of order  $\bar{I}^2$ , so we get a standard deviation of one point of the auto-correlation function of

$$\sigma \approx \frac{1}{\sqrt{K}} \sqrt{\frac{1}{\bar{I}^2} + \frac{6}{\bar{I}} + 5}. \quad (2.3.6)$$

So our result gets statistically better with  $\sqrt{K}$ , which is proportional to the square root of the experiment duration, for  $\bar{I} \ll 1$  (and this is generally the case in X-ray photon correlation spectroscopy) it gets better with  $\bar{I}$ , but it converges for high  $\bar{I}$ , there it is only determined by the finite experiment duration. Since we are more interested in the general shape of the auto-correlation function, i.e. the exponential coefficient, not so much in one point, we compute the correlation of two points

$$\frac{C_{\Delta k, \Delta l}}{\sqrt{V_{\Delta k} V_{\Delta l}}} = \bar{I}^4 \frac{1 + \bar{I}}{1 + 6\bar{I} + 5\bar{I}^2} \quad (2.3.7)$$

and see that for low count rates  $\bar{I}$  the correlation vanishes, so there is a considerable chance that the relative standard deviation of the fitted exponential factor also scales with the inverse of the square root of the number of significant points in the auto-correlation function, that is proportional to  $\sqrt{\frac{t}{\tau}}$ .

To arrive at an estimate for the relative uncertainty of the fitted exponential coefficient  $2\Gamma = 2(a - 1)st$  without taking into account finite coherence, background noise or inelastic scattering, finite exposure time or normalisation, we get

$$\sigma_{rel} \propto \frac{1}{\bar{I}\sqrt{K}} \sqrt{\frac{t}{\tau}} = \frac{1}{I_0\sqrt{tT}} \sqrt{\frac{t}{\tau}} = \frac{1}{I_0\sqrt{T\tau}} \quad (2.3.8)$$

with  $t$  the exposure time of one frame,  $I_0$  the expected count rate per second,  $K$  the number of frames and  $\bar{I} = I_0 \cdot t$  the expected count rate per frame and  $T$  the total duration of the experiment. This will only hold for small count rates  $\bar{I} \ll 1$  and for not too big  $\frac{\tau}{T}$ , an empirical rule being  $10^4$  correlation times  $\tau$  per experimental duration  $T$ , a rather big value. We have to remember once again that the uncertainty has two different roots: The first being Poisson noise, that is low intensities, and the second being the uncertainty of the evolution in the sample, that is the fluctuations in the expected instantaneous intensity. As the correlation time is governed by the temperature, ideally by an Arrhenius dependence, it is possible to set the correlation time to convenient values, where the optimal setting will be determined by the available beam intensity.

## 2.4 Normalisation

The aim of normalisation is to get the long-time limit of the auto-correlation function to be 1,  $\lim_{t \rightarrow \infty} g_2(t) = 1$ . The naïve way due to (2.2.5) would be to divide by the mean measured intensity. For low count rates and/or a low duration of the experiment in terms of the correlation time  $\tau$ , however, deviations are to be expected:

Since we compute the experimental auto-correlation function by

$$g_2(m) = \frac{1}{K - m} \frac{1}{C} \sum_n^{K-m} I_n I_{n+m} \quad (2.4.1)$$

and we want to have

$$EV(g_2(m)) = 1 + Ae^{-2\frac{m}{\tau}} \quad (2.4.2)$$

where we call  $A$  the measured contrast, we get

$$EV\left(\sum_n I_n I_{n+m}\right) = (K - m)C(1 + Ae^{-2\frac{m}{\tau}}). \quad (2.4.3)$$

Summing over  $k$  gives

$$EV\left(2 \sum_{m=1}^K \sum_{n=1}^{K-m} I_n I_{n+m}\right) = 2 \sum_{m=1}^K C(K - m)(1 + Ae^{-2\frac{m}{\tau}}). \quad (2.4.4)$$

## 2 Theory of photon correlation spectroscopy

The left side is equal to the expected value of  $(\sum_m I_m)^2 - \sum_m I_m^2$ , and after computing the sums on the right side we get an estimator for the normalisation factor

$$\frac{1}{C} = \frac{K(K-1) + 2A \frac{(K-1)\exp(2\Gamma) + \exp(-2\Gamma(K-1)) - K}{\exp(\frac{2}{\tau} - 1)^2}}{K^2 \langle I \rangle^2 - \sum_m I_m^2}, \quad (2.4.5)$$

where  $\langle I \rangle = \frac{1}{K} \sum_{m=1}^K I_m$  is our estimate for the mean instantaneous intensity.  $g_2(0)$  should give 2 by (2.2.5), but for low photon count rates Poisson statistics have to be taken into account, the effect of which we have already computed in (2.3.2), so we have to deal with it separately. To sum up, we see that since  $\langle I \rangle^2$  is given by the integral over the auto-correlation function, normalising by  $\langle I \rangle^2$  would get the mean of the auto-correlation function to be 1, not the long-time limit. This effect is especially prominent for short measurement times and low count rates.

Now we want to derive a lower bound (by neglecting the influence of photon noise) for the uncertainty of the normalisation: The covariance of two observed intensities  $I_k$  and  $I_{k+j}$  is given by

$$C_{k,k+j} = EV(I_k I_{k+j}) - EV(I_k) EV(I_{k+j}), \quad (2.4.6)$$

which is by (2.2.5) just  $N^2 e^{2-\frac{j}{\tau}}$  ( $\tau$  in terms of the frame duration), since this is exactly what the auto-correlation function measures. The variance follows trivially, so we have for the variance of the summed up intensity of  $K$  frames (frame duration  $T_f$ , mean expected intensity  $\bar{I}$ )

$$\sigma^2 = \bar{I}^2 t^2 \left( K + 2 \sum_{1 \leq i < j \leq K} e^{-2\frac{t}{\tau}|i-j|} \right). \quad (2.4.7)$$

We are only interested in a lower bound, so we take the optimal situation  $T_f \rightarrow 0$  where  $K \cdot T_f = T$  stays fixed, then the variance term vanishes and we have

$$\begin{aligned} \sigma^2 &= 2\bar{I}^2 \int_0^T dt \int_0^{T-t} dt' e^{-2\frac{t'}{\tau}} = 2\bar{I}^2 \int_0^T dt \frac{\tau}{2} (1 - e^{-2\frac{T-t}{\tau}}) \\ &= \bar{I}^2 \tau \left( T - \frac{\tau}{2} e^{-2\frac{T}{\tau}} (e^{2\frac{T}{\tau}} - 1) \right) = \bar{I}^2 \tau \left( T - \frac{\tau}{2} (1 - e^{-2\frac{T}{\tau}}) \right). \end{aligned} \quad (2.4.8)$$

The relative standard deviation is given by

$$\sigma_{\text{rel}} = \sqrt{\frac{\tau}{T} \left( 1 - \frac{\tau}{2T} (1 - e^{-2\frac{T}{\tau}}) \right)} \approx \sqrt{\frac{\tau}{T}}. \quad (2.4.9)$$

We see that the uncertainty here grows with larger  $\tau$ , in contrast to (2.3.8). Since this is just a lower bound, one obviously has to choose  $\tau$  about 2 orders of magnitude smaller than  $T$  to get a reasonable relative standard deviation, which is detrimental to (2.3.8).



What we have not considered yet is the possibility of averaging the auto-correlation function over a number of pixels. In a lattice one can not hope that the intensity evolutions at two different  $\Delta q$  have exactly the same statistical parameters, but since the deviations between neighbouring pixels are really small, definitely smaller than the expected uncertainty if we take just one pixel, it is a promising idea. There are two principal different ways of doing that: Firstly, averaging the unnormalised auto-correlation functions and then normalising (or not at all, allowing the baseline to be fitted as well), secondly, normalising the auto-correlation functions and then averaging. The first approach is (for small shift times) equivalent to longer measurement times with just one pixel (if the expected intensity is the same in each pixel averaged over), whereas the second will weight pixels with high intensity too little, so one can assume the first way to be the better one for small intensities. To arrive at a last estimate we get with (2.3.8) by averaging over  $M$  pixels

$$\sigma_{\text{rel}} \propto \frac{1}{I_0 \sqrt{MT\tau}}, \quad (2.4.10)$$

here we may also modify (2.4.9) to  $\sigma_{\text{rel}} \approx \sqrt{\frac{\tau}{MT}}$ .

In order to validate these considerations and to determine the proportionality factor, simulations will be carried out in the next chapter.

## 2.5 Non-ideal contrast

Until now we have assumed that everything is carried out under ideal circumstances, i.e. we have a fully coherent beam, the exposure time of one frame  $T_f$  is negligible compared to the correlation time  $\tau$  and we have no inelastic scattering or background radiation. Under these assumptions the estimated value of the pre-exponential factor in the auto-correlation function is unity. Now we are going to compute the effects of finite accumulation time, partial coherence and background radiation and see whether they may be neglected or have to be taken into account.

For computing the effect of finite accumulation time we denote the measured estimate of the auto-correlation function  $g_2(t)$  as  $g'(t)$  and have:

$$\begin{aligned} EV(g'(t)) &= \frac{1}{I_0^2} EV\left(\frac{1}{T_f} \int_0^T dt_1 I(t_1) \frac{1}{T_f} \int_t^{t+T_f} dt_2 I(t_2)\right) \\ &= \frac{1}{T_f^2} \int_0^{T_f} dt_1 \int_t^{t+T_f} dt_2 EV\left(\frac{1}{I_0^2} I(t_1) I(t_2)\right) \\ &= \frac{1}{T_f^2} \int_0^{T_f} dt_1 \int_t^{t+T_f} dt_2 g_2(t_2 - t_1) \\ &= 1 + \frac{1}{T_f^2} \int_0^{T_f} dt_1 \int_t^{t+T_f} dt_2 e^{-2\Gamma(t_2 - t_1)} \\ &= 1 + \frac{e^{2\Gamma T_f} - 1}{2\Gamma T_f} e^{-2\Gamma t} \frac{e^{-2\Gamma T_f} - 1}{-2\Gamma T_f} = 1 + e^{-2\Gamma t} \left(\frac{\sinh \Gamma T_f}{\Gamma T_f}\right)^2 \end{aligned} \quad (2.5.1)$$

## 2 Theory of photon correlation spectroscopy

This looks as if we can make the contrast arbitrary large by selecting big  $T_f$ . We have to keep in mind, however, that the first usable point in the measured auto-correlation function is at  $1 \cdot T_f$ , which goes faster to zero than the contrast rises. We cannot make  $T_f$  arbitrarily small because of the finite readout-times of detectors, but because of (2.4.10) we will use rather big correlation times  $\tau$ , so the modification can be kept negligible.

We also explore the case of an only partially coherent beam, e.g. because of a pinhole larger than the transversal coherence length, say  $H$  times as large, this is equivalent to considering the scattered amplitude of  $H$  samples summed, it is also equivalent to the case where the pixel size is  $H$  times the size of one speckle. In the following computation we are going to consider the last case, the scattering of  $H$  speckles, each with expected mean intensity  $\bar{I}$ , detected in one pixel, extended by the effect of a constant background radiation of  $c$  photons per frame. The probability density of  $k$  photons scattered into one speckle is given by

$$P(k) = \int_0^\infty dI \frac{1}{\bar{I}} e^{-\frac{I}{\bar{I}}} \frac{(I+c)^k}{k!} e^{-(I+c)}. \quad (2.5.2)$$

Since the amplitudes of the distinct speckles are per definition uncorrelated, the background radiation has no correlation whatsoever, too, we have for the unnormalised measured auto-correlation function:

$$\begin{aligned} Cg'(t) &= EV(I(0)I(t)) = EV\left(\sum_{i=1}^H I_i(0) \sum_{j=1}^H I_j(t)\right) \\ &= H(H-1)(\bar{I}+c)^2 + EV\left(\sum_{i=1}^H I_i(0)I_i(t)\right) \\ &= H(H-1)(\bar{I}+c)^2 + H(\bar{I}^2 g_2(t) + 2c\bar{I} + c^2) \\ &= (H(\bar{I}+c))^2 \left(1 + \frac{1}{H(\bar{I}+c)^2} \bar{I}^2 (g_2(t) - 1)\right) \\ &= (H(\bar{I}+c))^2 \left(1 + \frac{1}{H(1+\frac{c}{\bar{I}})^2} (g_2(t) - 1)\right), \end{aligned} \quad (2.5.3)$$

where we have made use of the fact that the expected value is linear and that the expected value of a product of independent random variables is the product of the expected values,  $I_i$  is the intensity of the distinct speckles and  $g_2(t)$  is the ideal auto-correlation function. We see that the measured autocorrelation function is undistorted, it has the same behaviour as the ideal auto-correlation function, the normalisation factor is given by  $(H(\bar{I}+c))^2$ , only the contrast  $A$  is diminished, it is given by  $A = \frac{1}{H(1+\frac{c}{\bar{I}})^2}$ , that means that it goes proportional to  $H^{-1}$ , but the dependence of the background radiation is  $(\frac{\bar{I}}{c})^2$ , it goes quadratically towards 0 when the background radiation is bigger than the elastically scattered intensity, but due to our crude estimate (2.4.10) we can hope that the standard deviation of the measured auto-correlation function only falls with  $c^{-1}$ , since the overall intensity (that is signal plus background) rises, which we will verify by simulations.

# 3 Simulations

## 3.1 Introductory simulations

With the above calculations, that is (2.1.35), it is possible to simulate XPCS experiments: First of all you define the lattice, the  $\Delta q$ -value you are interested in, the jump frequency  $s$ , the number of impurities  $N$ , the duration of the experiment  $T$  and the timestep  $t$  and use (2.1.4) to get an initial amplitude, and then you use (2.1.35)  $\frac{T}{t} = K$  times to get a sequence of expected amplitudes  $A_k$ ,  $0 \leq k \leq K$ . Then define  $I'_k = |A_k|^2$ ,  $0 \leq k \leq K$ , divide it by  $N$  (it should have mean value 1 now) and finally generate for each  $k$  a random number  $I_k$ , distributed according to Poisson with parameter  $I'_k$  times expected mean count rate. This recipe was already proposed in [Jakeman73] but is today not widely known, in fact it was developed independently for the thesis at hand and only found later.

For the following discussion we define the correlation time  $\tau = \frac{1}{(1-a)s}$ , such that the expected value of the auto-correlation function is given by  $g_2(t) = 1 + e^{-2\frac{t}{\tau}}$ .

Figure 3.1 is one realisation of the time evolution of the expected normalised intensity (before applying Poisson statistics) with contrast  $A = 1$ ,  $\tau = 100$  and 3000 frames.

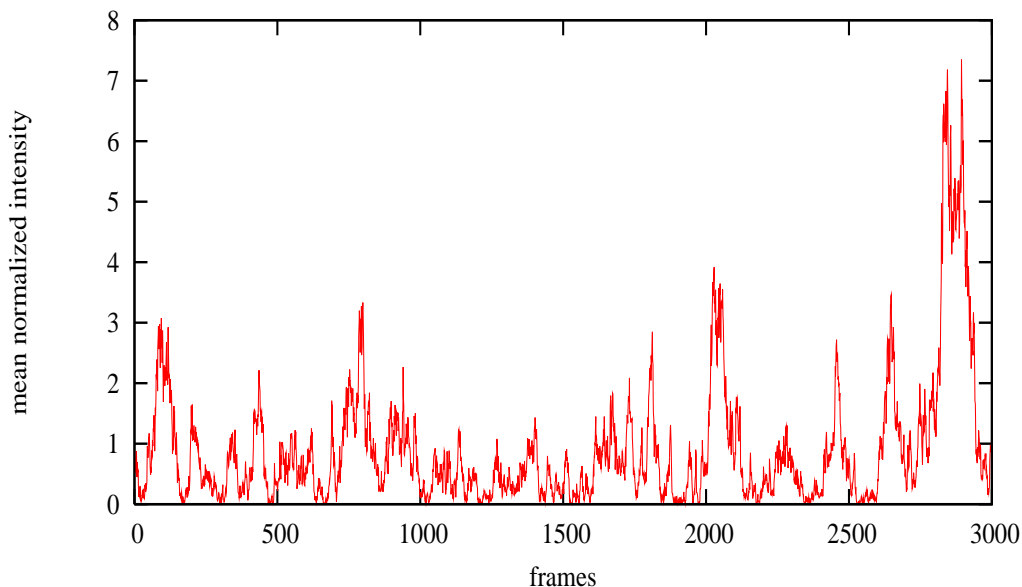


Figure 3.1: simulated time evolution of the normalised intensity,  $\tau = 100$

### 3 Simulations

The mean of this run is 0.905, which deviates just slightly from 1, in accordance with (2.4.9), the duration of the simulated experiment was just 30 correlation times. Figure 3.2 is a histogram of the above run, it should be exponentially distributed with mean 1, and figure 3.3 is its auto-correlation function, obviously 30 correlation times are far too less to make out a clear exponential decay, even without Poisson noise.

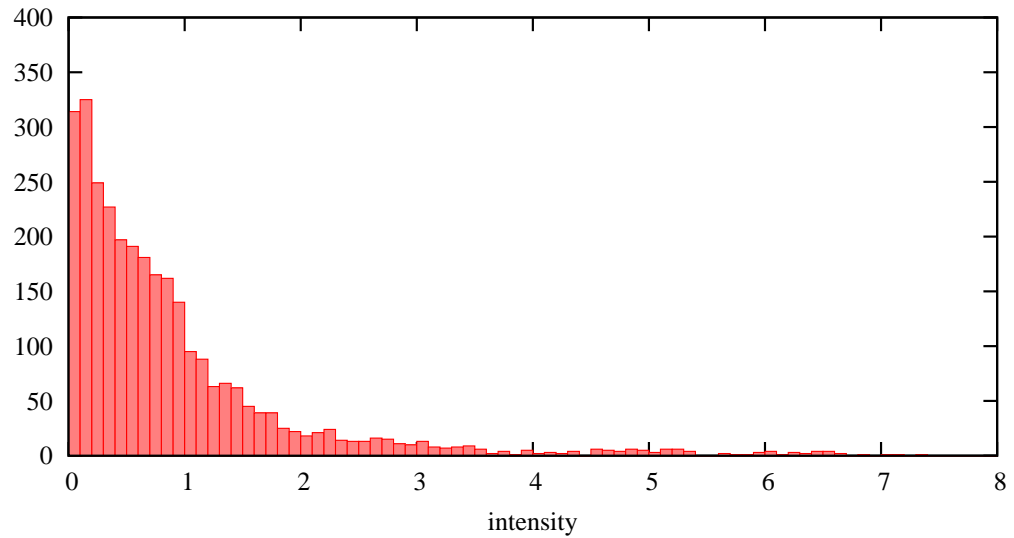


Figure 3.2: histogram of the normalised intensity,  $\tau = 100$

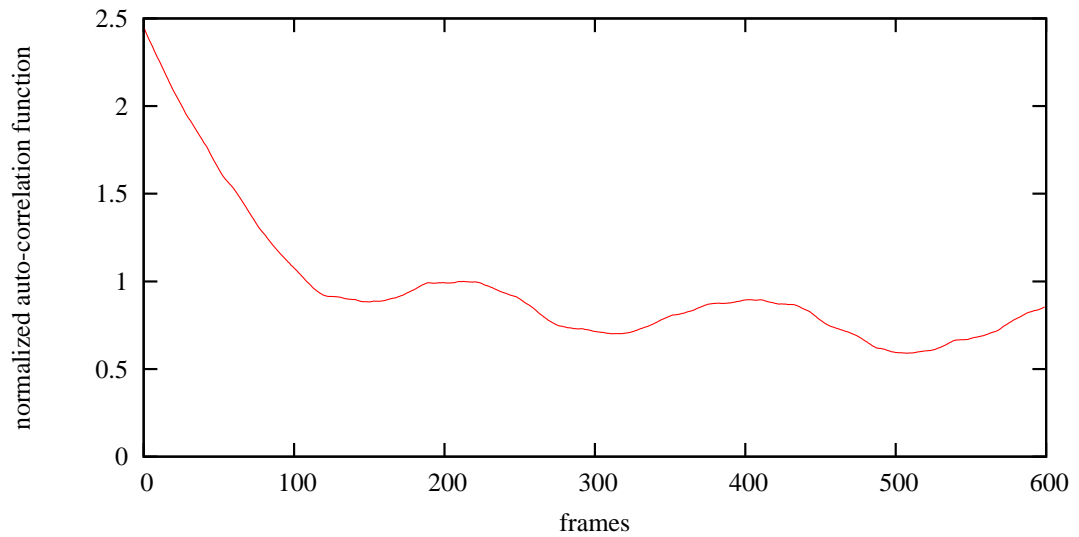


Figure 3.3: autocorrelation function,  $\tau = 100$

## 3.2 Verifying our estimates

For the following discussion we simulate experiments by taking  $M$  pixels, computing for each pixel a series of  $K$  non-negative integers  $I_k$  where  $EV(\sum_{k=1}^M I_k) = p$ , that is we fix the expected number of photons per pixel cumulated over the whole experiment, then computing the auto-correlation function for each pixel, averaging the auto-correlation functions over the pixels, and finally performing a least-squares-fit with the parameters  $A$ , the contrast, and  $2\Gamma$ , where  $\Gamma$  is the reciprocal value of the correlation time, that is  $g_2(t) = 1 + Ae^{-2\Gamma t}$ . We choose the normalisation to get the long-time-limit to be one rather than fitting it, for then we would have a third parameter, very much correlated with  $\Gamma$ , which would leave the fit less reliable. So we will use (2.4.5), rather just divide by the squared mean intensity, as it is commonly done, which would yield too short correlation times, especially at low intensity and low measurement times compared to  $\tau$ . As we have seen in 2.4, the correct normalisation depends then on the contrast  $A$  and on the correlation time  $\tau$ , that means, we need reasonable estimates on contrast and correlation time in order to normalise correctly. In a simulation, one knows the correct values beforehand, in reality this is not the case. A way out of this dilemma is a multiple-step-approach: First of all not normalising and fitting three parameters, then using the results, normalising and fitting two parameters and repeating the second step until it has converged. In general one will perform just a few fits for a few distinct situations (varying  $q$ , varying the temperature), therefore one can employ human intelligence to decide whether a fit is relevant or not, so there is no need for worrying about the implementation of the multiple-step-algorithm. In the simulations given here, many fits are performed, but here we know beforehand the correct contrast and correlation time. There are two possible ways of averaging, as we have seen in 2.4: weighting each pixel equally, that means normalising each measured auto-correlation function (in the following Method 1) or weighting according to the number of detected photons, that is summing all up and then normalising (Method 2). To make this clear, here is the procedure in pseudocode:

```

numpixel=100
numframe=1000
tau=50
p=40
f=2.5
auto1=zeros(1,f*tau)
auto2=zeros(1,f*tau)
normal2=0
for l=1:numpixel
    x=randn*sqrt(0.5)
    x=randn*sqrt(0.5)
    expint=x*x+y+y
    d=sqrt(expint)
    for k=1:anzframe

```

### 3 Simulations

```
    expx=d*exp(-1/tau)
    sigma=sqrt((1-exp(-2/tau))/2)
    x=randn*sigma+expx
    y=randn*sigma
    expint=x*x+y*y
    d=sqrt(expint)
    int(k)=poisson(expint*p/numframe)
end
auto1=auto1+autocorr1(int)
auto2=auto2+autocorr2(int)
normal2=normal2+normal(int)
end
auto1=auto1/numpixel
auto2=auto2/normal2
[A1 tau1]=expfit(auto1)
[A2 tau2]=expfit(auto2)
```

Here `randn` is a function that generates real normally distributed random numbers with expected value 0 and standard deviation 1, `poisson(x)` generates non-negative random integers with Poisson distribution with parameter `x`, `autocorr1(vector)` computes the auto-correlation function of the vectors of intensities `vector` and normalises it according to (2.4.5). `autocorr2(vector)` also computes the auto-correlation function, but does not normalise it, `normal(vector)` computes only the normalisation factor, and `expfit` performs a nonlinear least-squares fit  $f(k) \approx 1 + Ae^{-2\frac{k}{\tau}}$  by using the first  $f$  times  $\tau$  data points but omits the first, since this has at low count rates nothing to do with the real value, as we have already seen in 2.4. It returns the parameters  $A$  and  $\tau$ .

Figures 3.4 and 3.5 depict the situation for an expected value of overall 300 counts per pixel, figure 3.4 is a simulation of the number of incident photons in one single pixel at a correlation time of  $\tau = 100$ , the so-called photon bunching is clearly visible. Figure 3.5 is the corresponding measured auto-correlation function, averaged over 100 pixel. The fit (performed with GNU PLOT) returned a measured value for  $\tau$  of  $103.9 \pm 0.9$ . Figures 3.6 and 3.7 were obtained from a simulation with similar parameters but an expected value of only 30 counts per pixel, photon bunching is still visible, and the fit yields  $\tau = 110.5 \pm 8.8$ . In the latter case, one single point of the auto-correlation function has great uncertainty, but since the errors of the single points are apparently uncorrelated, a fit yields reasonable results. Also the estimated error is (especially for the former simulation) too low, which is not surprising since the fit is non-linear.

For the following simulations 200 runs of the above programme were performed for each parameter value, the error bars correspond to one standard deviation. The values for method 1 and method 2 are computed with the same vector of photon counts `int`, which explains the correlation between them.

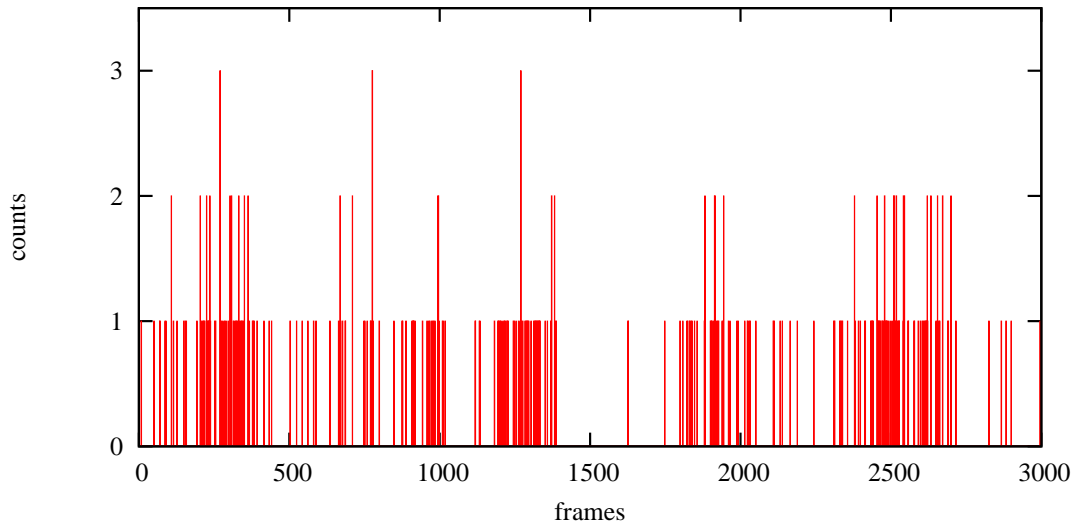


Figure 3.4: observed counts per pixel and frame (expected value 0.1)

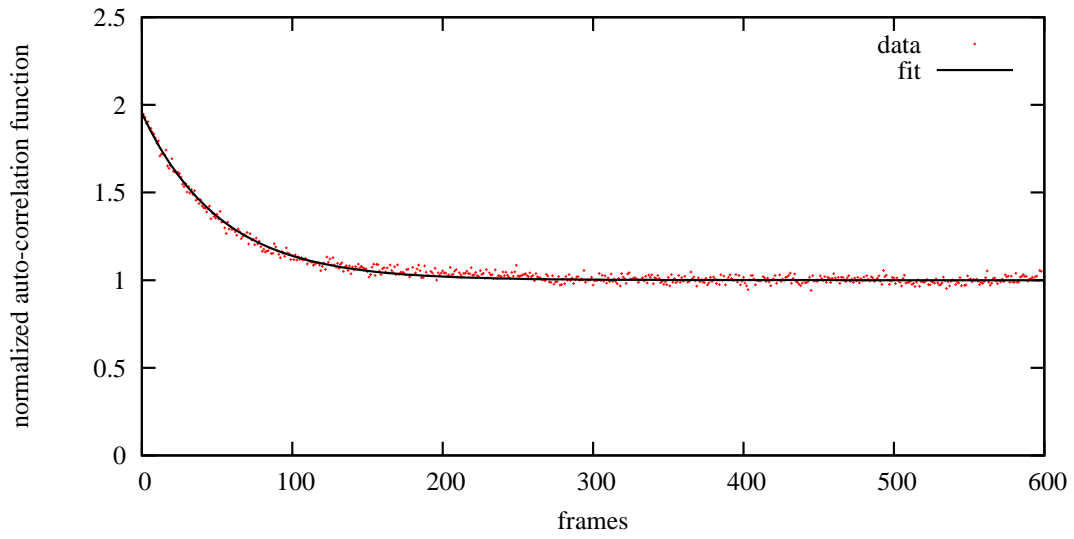


Figure 3.5: autocorrelation function with fit

### 3 Simulations

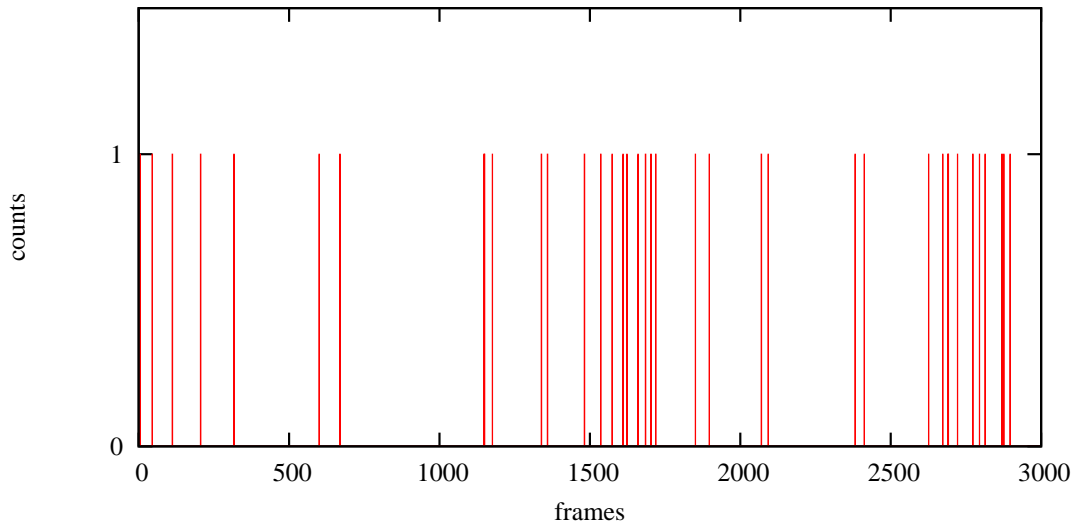


Figure 3.6: observed counts per pixel and frame (expected value 0.01)

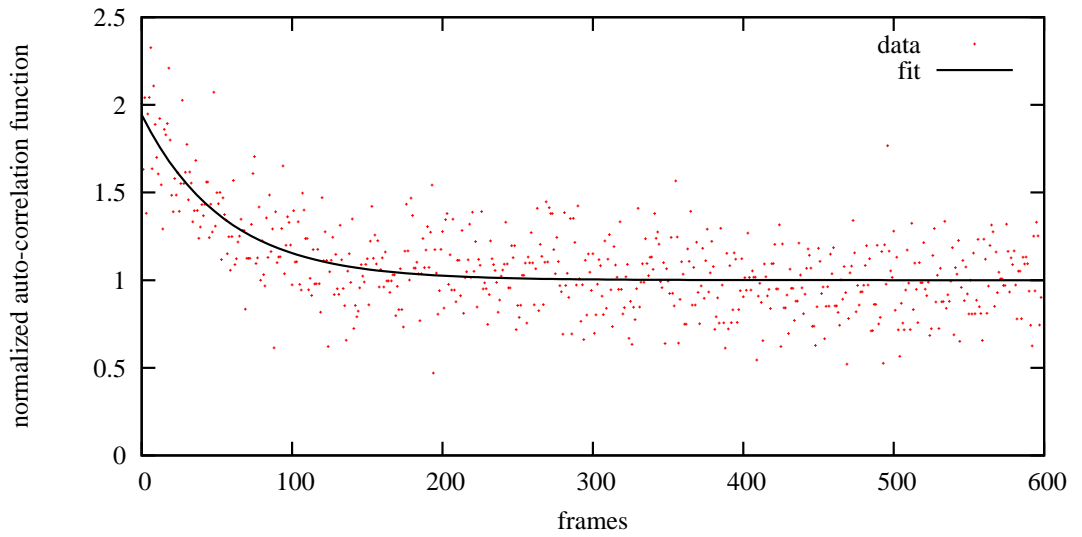


Figure 3.7: autocorrelation function with fit



### 3.2 Verifying our estimates

The first task is to decide on the range over which to fit the auto-correlation function. Clearly we have to exclude shift time 0. If we take the range too short, we lose significant points and we expect the signal-to-noise-ratio (SNR, we define it as the correct value of the correlation time divided by its uncertainty  $\frac{\tau}{\Delta\tau}$ , equivalently  $\frac{\Gamma}{\Delta\Gamma}$ ) to fall, for long times we have more computational expense and we possibly get a bias, supposing the normalisation is wrong and so the long-time-limit smaller than one, the fit will yield smaller correlation times and vice versa. Figure 3.8 shows the results for each value  $f$ ,  $f \cdot \tau$  being the number of frames over which the measured auto-correlation function was fitted, the parameters were  $M = 100$  pixels,  $K = 1000$  frames,  $\tau = 20$  correlation time (in units of frames) and expected counts per pixel over the whole duration of the experiment  $p = 50$ .

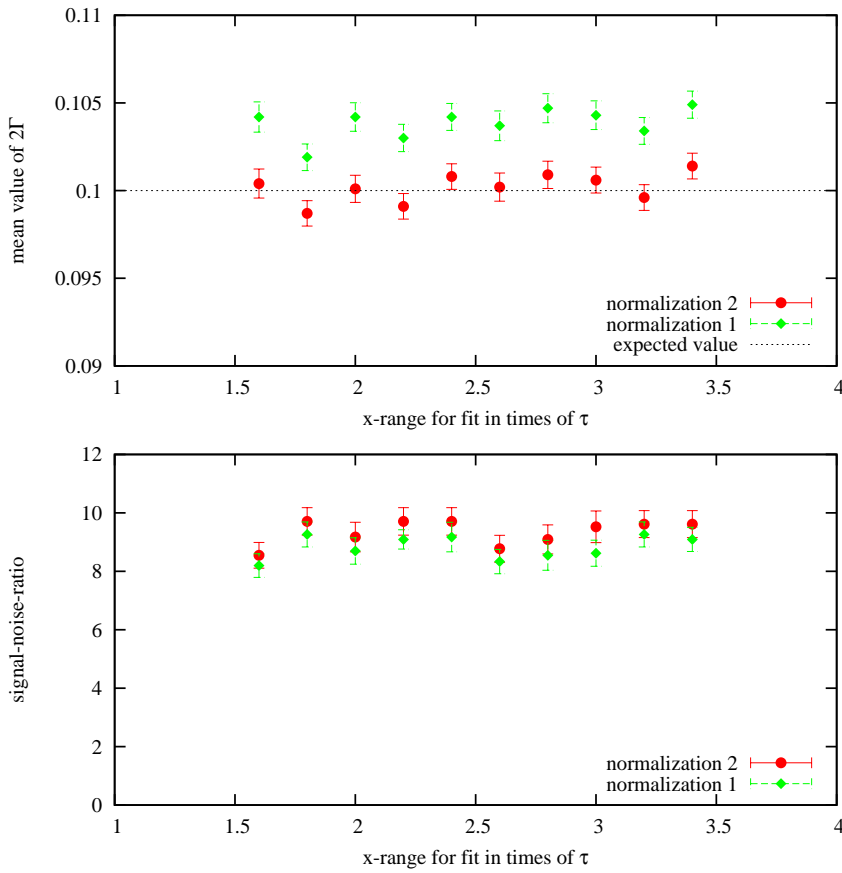


Figure 3.8: effect of varying the fit range

Since  $\tau$  was 20, we expect  $2\Gamma$  to be 0.1, obviously method 1 yields significantly too short correlation times, whereas the simulated SNR shows that method 2 is slightly better. It further seems as if all factors  $f$  used here yield the same results, so we take from now on  $f = 2.5$ .

### 3 Simulations

Now we want to verify that (2.4.10) is a function of the product  $M \cdot T$  only, that is averaging over more pixels cancels the effect of a shorter measurement time. We have again  $\tau = 20$  and we vary the number of pixel while keeping the product  $M \cdot T = 10^5$  fixed, also we keep the product  $p \cdot M$  fixed, that is we have a constant count rate, in accordance to the simulation above we fix  $p = 0.05T$ , see Figure 3.9.

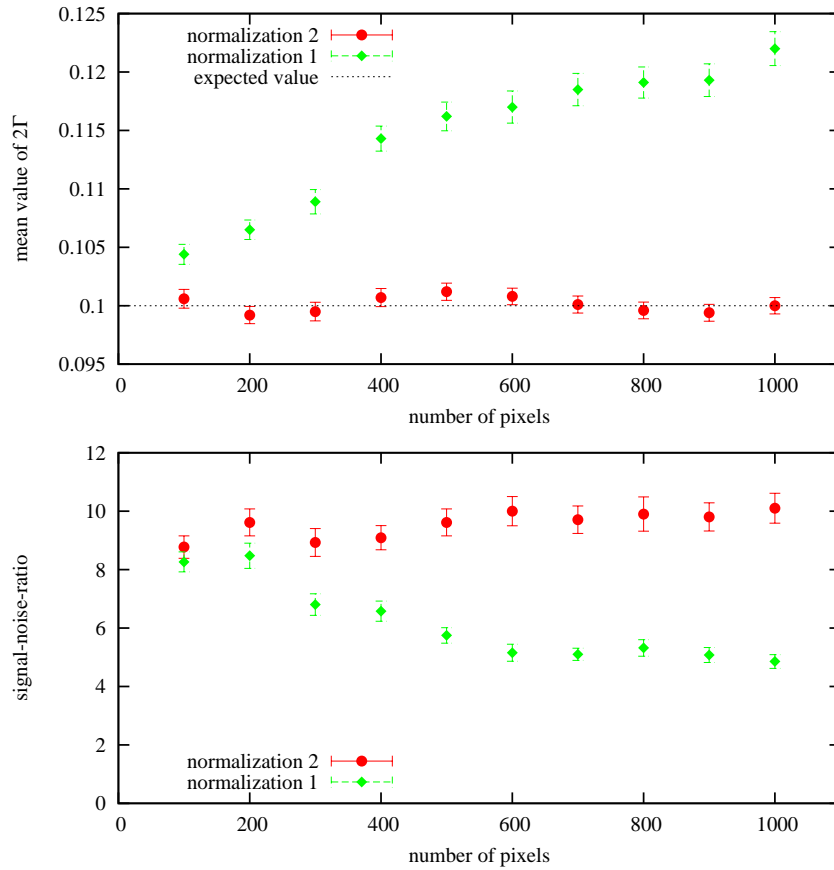


Figure 3.9: shorter experimental duration, more pixels and vice versa

We see that again method 1 yields too low correlation times, most pronounced at short experimental durations, whereas method 2 has no visible tendency, even at experimental durations of just 5 correlation times. Probably for method 2 the SNR slightly improves for short experimental durations and many pixels, whereas method 1 is considerably worse with decreasing experimental duration  $T$ , because the normalisation of the single auto-correlation functions to be averaged over becomes unstable.

### 3.2 Verifying our estimates

Remember that we are neglecting the effect of the finite accumulation time (duration of one frame), in our simulation we in fact implicitly assume that the expected intensity is constant during the accumulation time, which can only be valid if the accumulation time is short compared to the correlation time. Now we will check whether this simplification has distorted the outcome, so we will now divide our fixed experimental time into more and more frames at fixed total expected number of photons  $p$  and fixed correlation time in terms of the experimental duration:  $M = 100$ ,  $p = 50$ ,  $\frac{T}{\tau} = 50$ . Figure 3.10 displays the quantities renormalised to  $K_0 = 500$ .

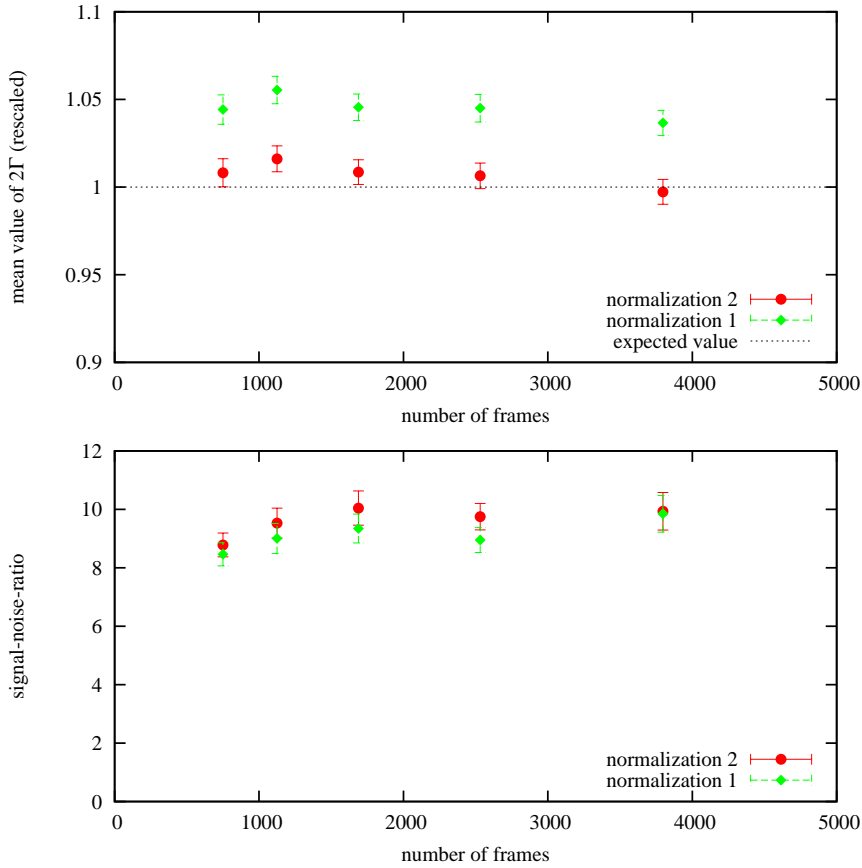


Figure 3.10: varying the accumulation time

As we have hoped, there is (at least for the mean) no visible tendency in the examined range.

### 3 Simulations

Now we want to determine the optimal correlation time  $\tau$ , since in the experiment we can choose the expected correlation time rather freely by adjusting the temperature. Again we take  $M = 100$ ,  $K = 1000$ ,  $p = 50$  and vary  $\tau$  (Figure 3.11).

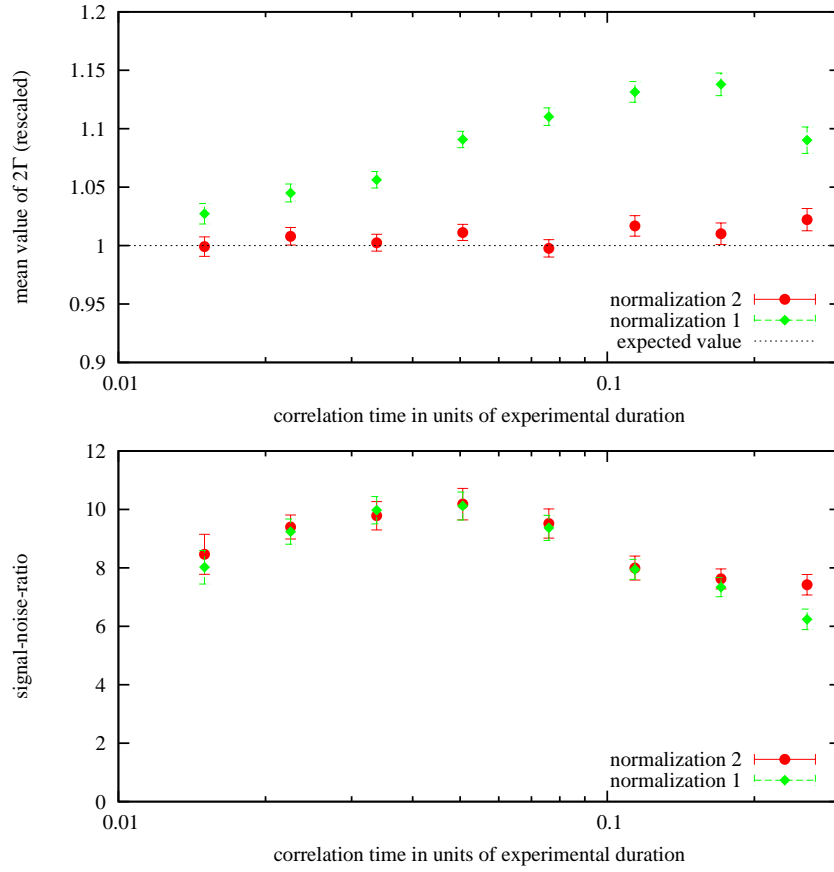


Figure 3.11: varying the correlation time

We see again that method 1 underestimates the correlation time systematically, most pronounced at long correlation times whereas method 2 has no tendency, so from now on we will consider method 2 superior in all relevant situations and drop method 1. It looks as if we have a range from 15 correlation times up to 50 correlation times where we have rather constant SNR, the predicted linear behaviour in  $\tau$  is not clearly visible.

To confirm above conclusion of the broad plateau with constant SNR, we repeat above simulations, but now we do not fit the auto-correlation function over the first  $2.5 \cdot \tau$  frames but we fix the upper limit at 250 frames, see figure 3.12.

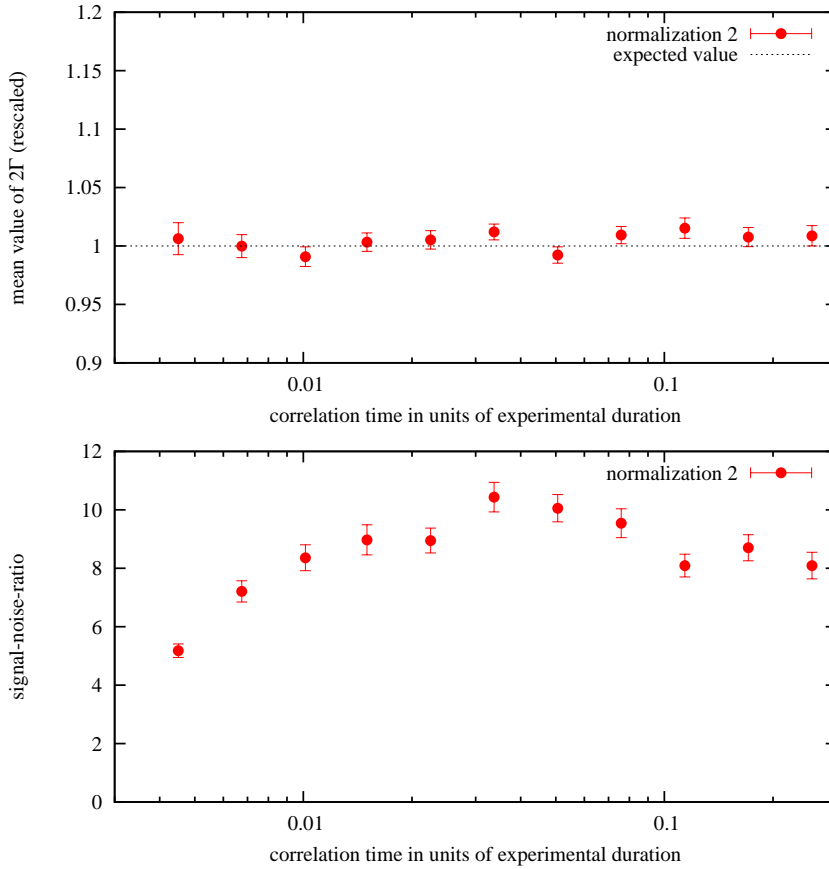


Figure 3.12: varying the correlation time again

Obviously the situation is the same, now we can also guess the linear behaviour of the SNR at (very) low  $\tau$ . This run would give for the proportionality constant in (2.4.10) a value of  $\approx 6.5$  in the linear region, but since one gets a better SNR with the same number of counts and experimental duration with longer correlation times, (2.4.10) is probably not so interesting, we try another estimate for the SNR at its peak

$$\text{SNR} \approx rp\sqrt{M}, \quad (3.2.1)$$

where  $p$  is the mean number of photons per pixel over the whole experimental duration,  $r$  is an empiristic proportionality constant, with this run we have  $r \approx 0.02$ , the peak is at about 20 correlation times per experimental duration.

### 3 Simulations

We are still at rather high counts, so we will now try to decrease the counts and cancel the expected loss in SNR by averaging over more pixels: We take  $K = 1000$ ,  $\tau = 50$  and keep the product  $p^2 \cdot M = 250000$  fixed:

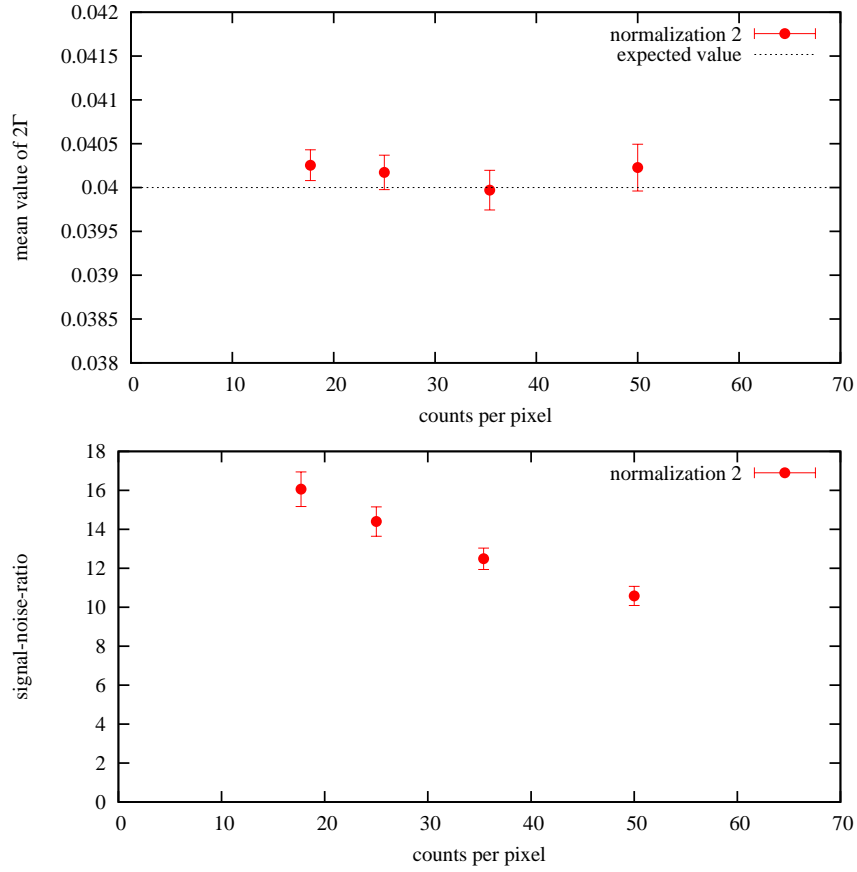


Figure 3.13: compensating low counts with many pixels

The SNR behaves better than predicted at low count rates, the probable answer is that the overall SNR has contributions from (2.3.8) and (2.4.9), where we only expect the former to be constant at constant  $p^2 \cdot M$ , the latter clearly gets smaller. This is also a hint that the peak in the SNR (as a function of  $\tau$ ) has shifted to larger  $\tau$ , which we will explore later.

### 3.2 Verifying our estimates

The above run has yielded really high SNRs at low counts, so we have room to decrease the number of counts further, so now we try  $M = 2500$ ,  $K = 200$ ,  $\tau = 10$  (which corresponds to the position of the peak at rather high counts) and vary the mean counts per pixel summed over the whole measurement time:

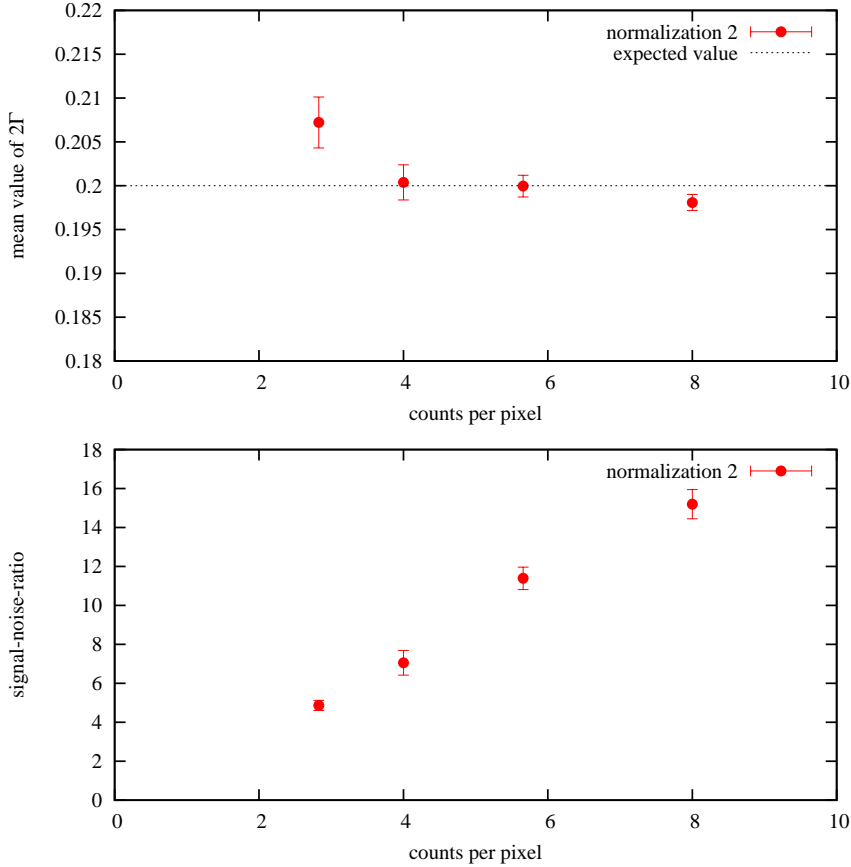


Figure 3.14: going towards very low counts

Now it seems like  $r \approx 0.035$ , also a test run with the same  $M$  and  $K$  as above, but with  $\tau = 20$  and  $p = 2.83$  (the smallest value in the run above) gives a SNR of 8.16, which means an  $r$  of at least 0.058. So it is obvious that the position of the peak of the SNR depends on the number of counts, at low counts longer correlation times give better results. Also it seems like that the SNR was at 100 pixels still restricted by the finite number of correlation times averaged over (because  $r$  got so much better, see (2.4.9)). If the outlier at 2.8 counts per pixel is of statistical or systematic nature, we have yet to further investigate.

### 3 Simulations

To find the optimal value for  $\tau$  in terms of the experimental duration, we keep the above values ( $M = 2500$ ,  $K = 200$ ,  $p = 2.83$ ) and vary  $\tau$ :

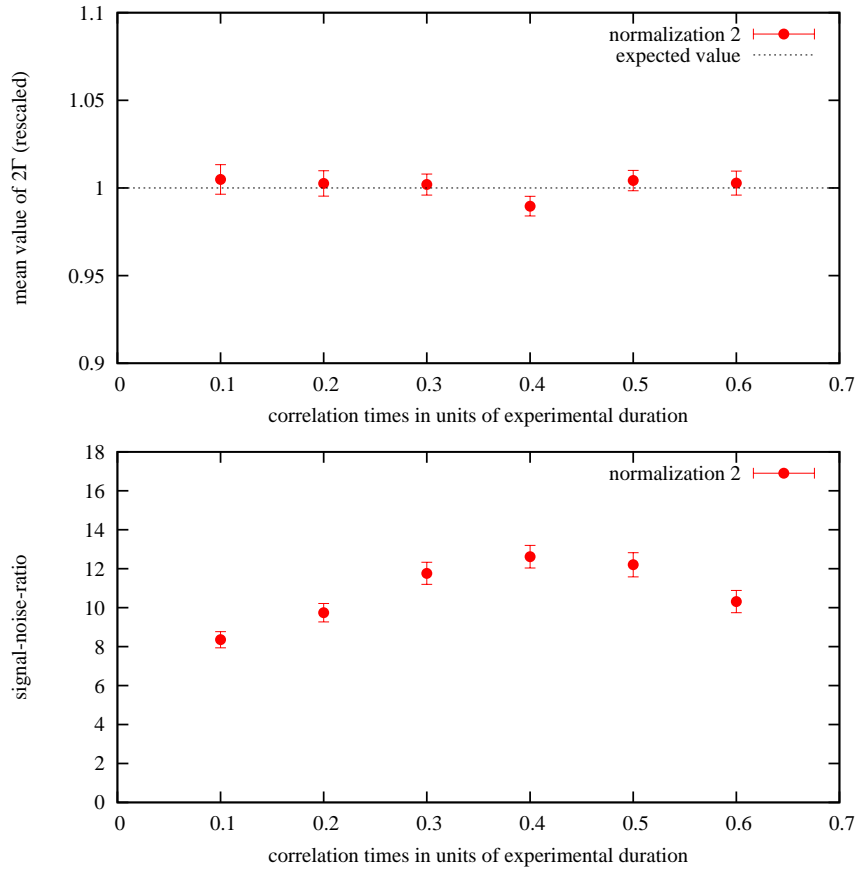


Figure 3.15: finding the peak of the SNR

This time there are no deviations in the mean correlation time (so we can answer the above question about the nature of the outlier in favour of a statistical nature), and the best SNR for  $\tau = 80$ , that means just 2.5 correlation times per experimental duration. Here we have a value  $r \approx 0.088$ , so apparently the linear range, where (2.4.10) holds, expands with decreasing count rate and increasing number of pixels averaged over, until it eventually comprises the whole experimental duration  $T$ , because if we set  $\tau = T$  in (2.4.10), (3.2.1) follows. We have to keep in mind that in real-life experimentation the beam or the sample can move, obviously all correlation is lost after such an event, which means the overall experimentation time decomposes into smaller actual experimentation times. Therefore it is really not wise to choose the expected correlation time in the order of hours, but rather (e.g.) about a factor two smaller than the expected mean time between two above mentioned correlation losses (if we have a clue what time this will be).



Still left to validate are the results of 2.5. Again with the same values as above ( $M = 2500$ ,  $K = 200$ ,  $p = 2.83$ ,  $\tau = 80$ ) we simulate this time the effect of larger pixels than speckles by summing a number of uncorrelated instantaneous intensities and then applying Poisson statistics. As always, the mean correlation time shows no deviations from the predicted value, so we make room for the contrast:

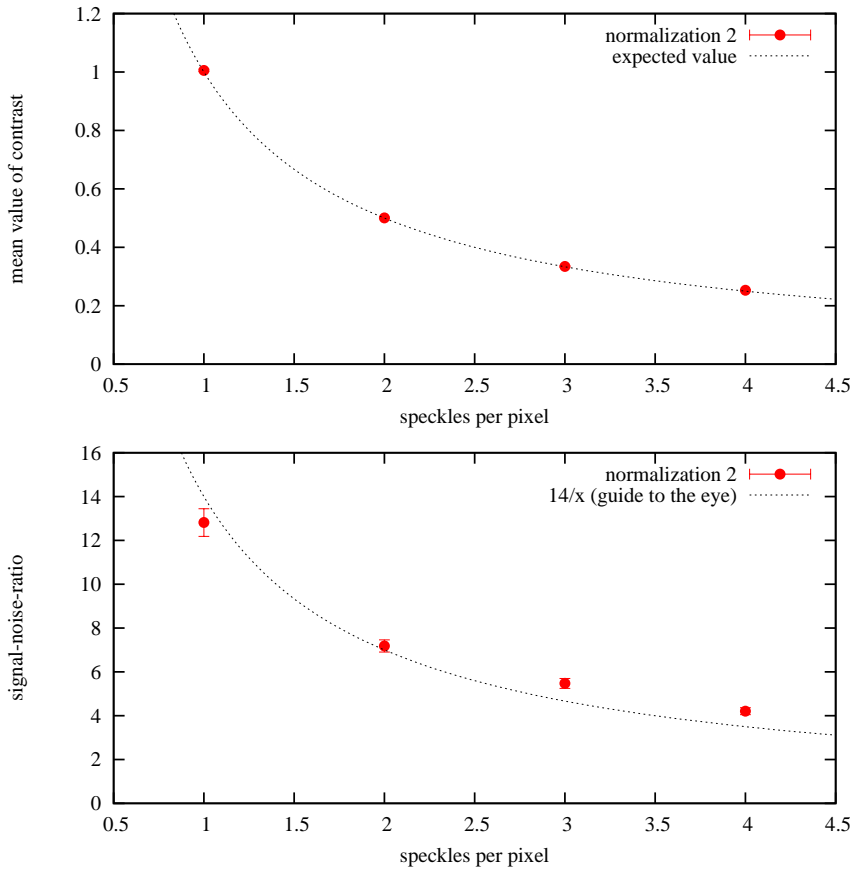


Figure 3.16: averaging over speckles

The contrast behaves just as predicted (the error bars are smaller than the point size), whereas the SNR behaves better than one would presume (i.e. the standard deviation rises slower than the contrast falls,  $14/x$  being just a guide to the eye), a possible explanation would be that even at this low count rate (2.4.9) still affects the SNR, which gets better with more speckles averaged over.

### 3 Simulations

Now to the effect of (uncorrelated) background radiation: With still the same values as above ( $M = 2500$ ,  $K = 200$ ,  $p = 2.83$ ,  $\tau = 80$ ) we add background photons with mean count rate  $p_b$ :

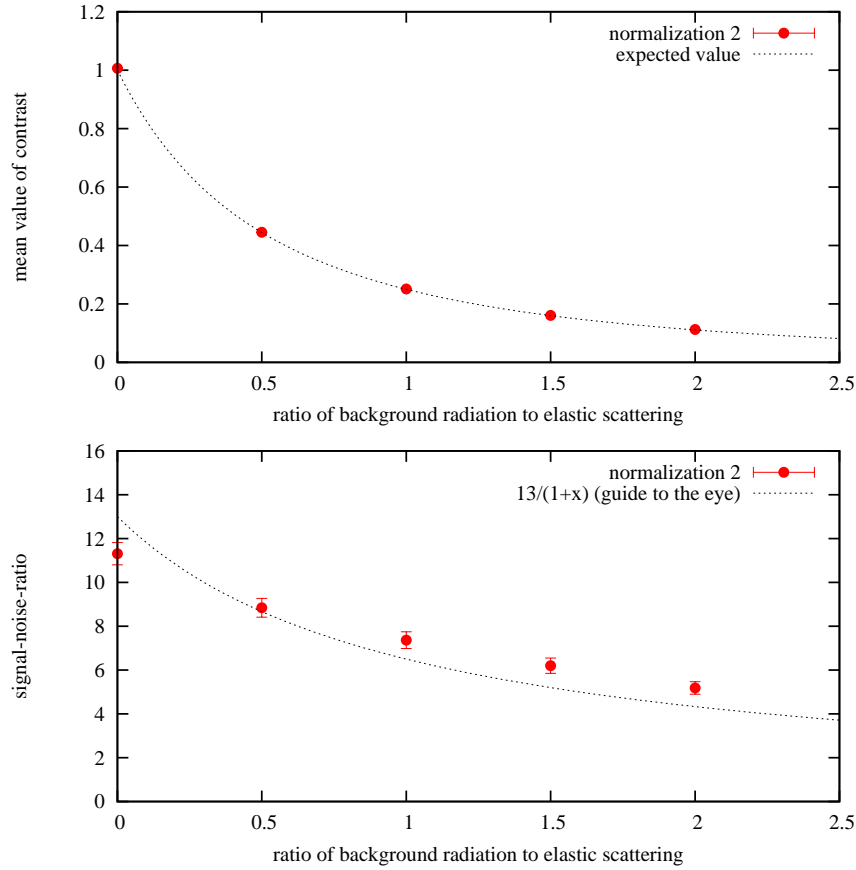


Figure 3.17: effect of background radiation

We see that the contrast behaves exactly as predicted (again the error bars vanish), whereas the SNR goes slower towards zero than  $1/(1 + \frac{p_b}{p})$ , which is sketched by the dotted line. Even if the background radiation is  $\frac{2}{3}$  of the overall intensity, the SNR just drops by a factor of 2.

### 3.3 Conclusion

Recapitulating the above results, by choosing the correlation time wisely, we can have for 2500 pixels to be averaged over and 2.8 counts per pixel over the whole experimental duration a SNR of about 12 under ideal circumstances, if we assume instabilities of the beam or the sample, we should choose the correlation time shorter, about one half or less of the expected time of stability, and we can expect a reduction of the SNR

by a factor of the square root of the number of correlation losses (since then we have to consider an actual pixel as different before and after the correlation loss, so we have more virtual pixels, but less counts per virtual pixel). Non-ideal coherence also reduces the SNR, but as we have seen, estimating the reduction of the SNR by the coherence factor is really conservative. If we have background radiation, we have again a very conservative estimate of the SNR, it reduces with a factor one plus the ratio of background scattering (or inelastic) to elastic scattering. When measuring away from Bragg peaks and unless for really small  $\Delta q$ -values, 2500 pixels should be available with almost the same expected underlying dynamics, so five counts per pixel should give statistically rather good results, even with realistic coherence factors and background radiation. If the count rate is lower, one can keep the SNR with a quadratical increase of the number of pixels considered, which is again a conservative estimate, see Figure 3.13.

### 3 Simulations

## 4 Optimising the beamline-setup

In the above chapters we have derived an estimate for the signal-to-noise-ratio, that is we want to maximise the product of contrast and intensity per pixel (as long as we stay at low intensities). Contrast and intensity are functions of beamline design, some user-adjustable settings, of the sample and the detector. Now we want to talk about the optimisation of the beamline-settings. We will take as an example the specifications of the beamline ID10A at the ESRF (European Synchrotron Radiation Facility) in Grenoble, France [TRO].

### 4.1 Fundamental layout

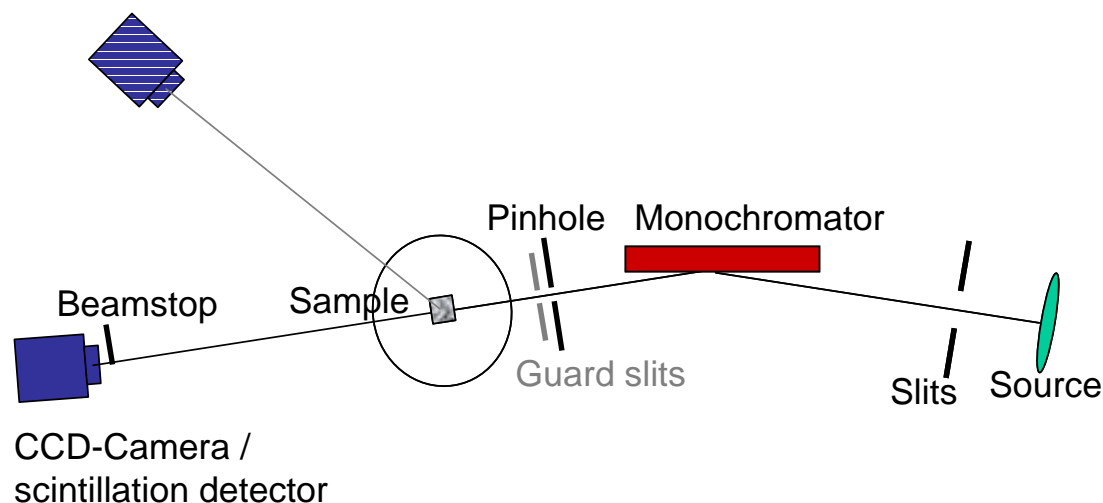


Figure 4.1: schematic layout of a beamline, taken from [Stadler06a]

The X-ray radiation is generated by electrons circulating in the synchrotron ring at relativistic velocities passing an undulator, which is a sequence of strong magnets with alternating polarity. By Lorentz' law the electrons are accelerated perpendicularly to their propagation direction and emit radiation which is polarised parallel to the acceleration, i.e. they are polarized in horizontal direction. Due to the relativistic velocities the radiation is nearly totally emitted into forward direction [Als-Nielsen01]. The electron bunch is not circular, rather elliptical, with the longer axis in the horizontal direction, so the source of the radiation is also elliptical (in fact it is commonly modelled by a product of a Gaussian in horizontal direction and one in vertical direction, the

## 4 Optimising the beamline-setup

size being defined as the full width at half-maximum of these Gaussians), at the ESRF the size is given by  $\sigma_x = 928\mu\text{m}$  in the horizontal direction,  $\sigma_z = 23\mu\text{m}$  in the vertical direction. The source size is of importance, as we are going to see, to make a long story short, the more circular, the better. One way to overcome this obstacle is focussing, at ID10A there exists the possibility of vertically focussing, either by beryllium lenses or by a thermally bended mirror. By focussing we get an image (of a certain size at a certain position) of the source, and we can treat this image as a new source with the same brilliance as the actual source, where brilliance is defined as the number of photons per second, per solid angle in  $\text{mrad}^2$ , per one  $\text{mm}^2$  source size, and per 0.1% bandwidth. So the actual source size is not of importance, everything we need to know is the angular source size  $\vartheta_x \times \vartheta_z$  as seen from the sample (resp. the angular source size of the image), and we shall not forget that we can choose the angular source sizes between reasonable bounds by focussing with constant brilliance. After focussing the beam is monochromatised by reflecting it on a monocrystal (there is a number of them at hand, so the temporal coherence can be set in steps from  $2.31 \times 10^{-5} < \frac{\Delta E}{E} < 1.428 \times 10^{-4}$ ), and immediately upstream of the sample the beam is passed through an adjustable pinhole, for the sake of simplicity we only consider rectangular pinholes ( $L_x \times L_z$ ). In fact roller-blade slits have been available for defining the beam at the TROIKA beamline for a short time now. We now assume that this yields an illuminated area on the sample of  $L_x \times L_z$ , that is that we are not in the region of Fraunhofer scattering, whether this assumption holds, we have to think about later.

### 4.2 Contrast and intensity

This section is based heavily on [Falus06], but comes to other conclusions because of focussing being taken into account.

We define  $\omega_x \times \omega_z$  the angular size of one pixel as seen from the sample, and due to [Mochrie00] we define the effective coherence length in the horizontal direction as

$$\Xi_x = \frac{\lambda\sqrt{8\ln 2}}{2\pi} \frac{1}{\sqrt{\omega_x^2 + \vartheta_x^2}}, \quad (4.2.1)$$

the effective coherence length in the vertical direction  $\Xi_z$  is defined analogously.

Due to [Sandy99], we may approximate the overall optical contrast  $A$  as some integral of a product of a longitudinal (i.e. energy-resolution dependent) and a transversal factor. Further we may approximate this integral of a product as a product of the corresponding integrals (this is a conservative estimate because the two factors have a positive correlation coefficient). Now we are going to treat the longitudinal factor, which is given by

$$\frac{1}{V^2} \int_V d\mathbf{r}_1 \int_V d\mathbf{r}_2 e^{(-\delta(\mathbf{r}_1, \mathbf{r}_2)/\Lambda)}, \quad (4.2.2)$$

for a Lorentzian power spectrum of the beam (which is the case after reflection on a monochromator) the longitudinal coherence length is given by  $\Lambda = \frac{\lambda}{\pi} \frac{E}{\Delta E}$ , and the

path-length difference is given by

$$\delta(\mathbf{r}_1, \mathbf{r}_2) = |x_1 - x_2| \sin(2\theta) + |y_1 - y_2|(1 - \cos(2\theta)) \quad (4.2.3)$$

when measuring in the horizontal plane. In transmission geometry, the illuminated volume is given by  $L_x \times L_z \times W$ , so the distribution of possible path-length differences is a trapezium with parallel sides

$$a_1 = L_x \sin(2\theta) + W(1 - \cos(2\theta)) \quad (4.2.4)$$

and

$$a_2 = L_x \sin(2\theta) - W(1 - \cos(2\theta)) \quad (4.2.5)$$

for small  $\theta$ , and (4.2.2) is given by

$$\int d\delta p_{\text{PLD}}(\delta) e^{-\frac{\delta}{\lambda}}, \quad (4.2.6)$$

where  $p_{\text{PLD}}(\delta)$  is defined as

$$p_{\text{PLD}}(\delta) = \begin{cases} \frac{4}{a_1 + a_2} & 0 < \delta < \frac{a_2}{2} \\ \frac{4(a_1 - 2\delta)}{(a_1 - a_2)(a_1 + a_2)} & \frac{a_2}{2} < \delta < \frac{a_1}{2} \\ 0 & \text{elsewhere} \end{cases} . \quad (4.2.7)$$

One has to remember that this estimate only considers the loss of coherence of the scattered radiation due to path-length differences, the same effect is used when measuring the longitudinal coherence length with a Michelson-interferometer. Not considered is the loss of coherence due to a smearing out of the speckles in radial direction. Since the energy distribution of the incident beam is finite, one detector pixel (that is one distinct value of  $2\theta$ ) corresponds to a distribution of values of  $\Delta q$  with the same relative width. For a rough estimate the size of the speckles in  $q$ -space is given by  $\frac{1}{L_i}$ , where  $L_i$  is the corresponding dimension of the scattering volume in real space, so the number of speckles averaged over is given approximately by  $\frac{\Delta E}{E} \Delta q L$ . Due to our considerations in 2.5 the relevant factor for the contrast is given by the inverse of the number of speckles averaged over, and it turns out that this effect is roughly of the same order as 4.2.2. An important consequence is the elongation of speckles in radial direction (reported for example in [Sandy99]). So if the contrast suffers due to big scattering angles, there is the possibility of binning several pixels together (in radial direction), so the mean count rate per binned pixel rises, the number of pixels drops, which is an overall gain in signal-noise-ratio of the square root of the number of pixels binned together.

Again due to [Mochrie00] the transversal factor factorises in a horizontal and a vertical term,

$$A \approx F(L_x/\Xi_x)F(L_z/\Xi_z), \quad (4.2.8)$$

#### 4 Optimising the beamline-setup

where  $F$  is given by

$$F(x) = \frac{1}{x^2}(x\sqrt{\pi}\operatorname{erf}(x) + e^{-x^2} - 1). \quad (4.2.9)$$

$\operatorname{erf}(x)$  is the error function, it is defined as

$$\operatorname{erf}(x) = \frac{2}{\sqrt{\pi}} \int_0^x e^{-t^2} dt. \quad (4.2.10)$$

This holds for small  $2\theta$ , for larger values the speckles get smaller and so the contrast is diminished, but the whole estimate is very conservative regarding the pixel size (see [Mochrie00], equation (A9)).

With the brilliance  $B$  we have the number of incident photons per second and  $\text{mm}^2$

$$\phi = B \frac{\Delta E}{E} \vartheta_x \vartheta_z \frac{2\pi}{8\ln 2}, \quad (4.2.11)$$

the numerical factor is the consequence of defining  $\vartheta$  via the full width at half-maximum rather than the standard deviation. For optimising the beamline-setup we now neglect the dependence on longitudinal coherence (we have to care about that when evaluating possible samples). At low intensities the signal-to-noise ratio is proportional to the product of contrast  $A$  and mean count rate per pixel  $I_0$  times the number of pixel (which is fixed), so we have

$$\text{SNR} \propto I_0 A \propto \omega_x \omega_z \phi L_x L_z F(L_x/\Xi_x) F(L_z/\Xi_z). \quad (4.2.12)$$

We see that above equation factorises into a horizontal and a vertical term, so we seek to maximise them independently and define a quantity proportional to our expected SNR (per dimension)

$$r_{\text{sn}} = \omega \vartheta L F(L/\Xi), \quad (4.2.13)$$

and we have

$$r_{\text{sn}} = F\left(\frac{L}{\Xi}\right) \omega \vartheta \Xi \frac{L}{\Xi} \propto F(x) x \frac{1}{\sqrt{\frac{1}{\omega^2} + \frac{1}{\vartheta^2}}}, \quad (4.2.14)$$

where the proportionality factor is just the wavelength and a numerical constant, and we see that after having chosen  $\omega$  and  $\vartheta$  we have left  $L$  to set  $x$  where we want. For large  $x$ ,  $F(x)$  is given by  $F(x) \approx \frac{\sqrt{\pi}}{x}$ , which can be verified by Taylor expansion, whereas it converges for small  $x$ , also  $F(x) \cdot x$  is monotonically increasing and concave, so to make it large, one has to choose large  $x$ , i.e. large pinhole diameters (in terms of the effective coherence length), but not too large, since then the SNR does not increase linearly with the count rate any more, whereas the contrast vanishes. Also we see that the bigger the angular pixel size and the angular source size, the better. However, it doesn't improve the situation any more when one factor is much bigger than the other.



Let us reflect on that a little: the common way (without focussing) is having some fixed source size (very elliptical), then adjusting the pinhole to a few coherence length's width and height (optimally much higher than wide due to the respective coherence lengths), a common value for the contrast is  $A = 0.2$ . Then one chooses the detector position such that one pixel is not much bigger than one speckle. Since the speckles' dimensions are given by the reciprocal dimensions of the pinhole and the beam-defining slits, respectively, the speckles are not necessarily circular, but this can be overcome by binning several pixels together (summing up their intensities when evaluating the data). The approach chosen here relies on focussing, which makes the source sizes virtually arbitrary (at constant brilliance). One can increase the flux by increasing the source size, that also decreases the coherence lengths, which has to be countered by making the pinhole small, so one has a fixed number of photons per coherence length, that is a fixed number of coherent photons, but one can choose the beam diameter. Since the angular extent of one speckle is given by the extent of the illuminated volume, one can make the speckles rather big by making the beam diameter small, the whole process at constant contrast and constant scattered photons per unit angle, so the number of photons per speckle rises, which is the relevant quantity for the signal-to-noise ratio.

Now for actual values back to ID10A: As the horizontal source size is  $\sigma_x = 928 \mu\text{m}$  and no horizontal focussing is possible, we have a horizontal angular source size (at a distance of the sample  $R = 46 \text{ m}$ ) of  $2.0 \cdot 10^{-2} \text{ mrad}$ , by vertical focussing we can also get a vertical angular source size of this order. So we will need angular pixel sizes of at least this order, thus (since the detector in use has pixel dimensions of  $(20 \mu\text{m})^2$ ) a detector-sample-distance of about 1 meter. Operating at 8 keV, this gives an effective coherence length of  $2.04 \mu\text{m}$ , so for a reasonable contrast we will have to choose our pinhole rather small, let's say  $(4 \mu\text{m})^2$ , which yields a value of  $F(1.96) = 0.64$  per dimension. Due to (4.2.11) and by assuming a peak brilliance  $B > 10^{20}$  photons per second, per solid angle in  $\text{mrad}^2$ , per one  $\text{mm}^2$  source size, and per 0.1% bandwidth at 8 keV at 100 mA ring current we have  $\phi = 7.5 \cdot 10^{15}$  photons per second and  $\text{mm}^2$  at  $\frac{\Delta E}{E} = 1.428 \cdot 10^{-4}$  (but only during the peaks!), that is we have a theoretical incident beam of  $1.2 \cdot 10^{11}$  photons per second with transversal coherence factor of 0.47 and a longitudinal coherence length of  $0.35 \mu\text{m}$ . Losses at mirrors and monochromator are here disregarded, also the peak intensity is only of theoretical value, but the reported common value (without focussing) of about  $2.7 \times 10^9$  photons per second through a  $10 \times 10 \mu\text{m}^2$  pinhole allows us to arrive at a realistic estimated value of  $1.7 \times 10^{10}$  photons per second (we propose a 40 times larger effective source size and a 6.25 times smaller pinhole). We have chosen our pinhole very small, which is only sensible if the beam spot on the sample is not wider than the pinhole, because actually it is the size of the beam spot on the sample that determines the size of the speckles and hence the coherence factor. With the common criterion for non-Fraunhofer diffraction ( $\lambda R \ll d^2$ ,  $R$  is the distance of aperture to screen,  $d$  the width of the slit) one would need in our case a pinhole-to-sample distance of much less than 10 cm at 8 keV. Exact calculations show that the first effects of a widening of the beam occur at a distance of about 11 cm, where the smallest possible sample-to-detector distance at ID10A seems about to be 7 cm. Clearly bigger pinhole sizes would give a higher count rate at lower contrast, due

#### *4 Optimising the beamline-setup*

to the above estimates the SNR would even rise, but in order to have comparably high contrasts we now keep the slit sizes at  $(4\mu\text{m})^2$ , if there arise technical problems with this setting, we can raise this value without problems.

# 5 Optimising the sample

This chapter will present some really basic properties on the interaction of X-rays with matter in order to specify desirable properties of samples to be investigated with XPCS. There are other mechanisms of interaction, but for the photon energies at hand these are negligible, for a profound treatment see [Als-Nielsen01]. We will then compare some potential systems and decide on the feasibility of detecting diffusion on atomic scale.

## 5.1 Interaction of X-ray photons with matter

### Elastic scattering

By Maxwell's laws, an incoming electromagnetic wave forces a free electron to oscillate, so we have an accelerated charge equivalent to a dipol antenna, which acts itself as a source of an emitted electromagnetic wave. This emitted wave has clearly the same frequency as the stimulant wave, so the corresponding photons have the same energy, therefore the process is called elastic scattering. Also one expects an angular dependence. By doing the calculation, one arrives at the differential cross section per electron

$$\left(\frac{d\sigma_{\text{el}}}{d\Omega}\right) = r_0^2(\sin 2\theta)^2, \quad (5.1.1)$$

where  $r_0$  is the so-called classical electron radius, also Thomson scattering length, in SI-units we have  $r_0 = \frac{e^2}{4\pi\epsilon_0 mc^2} = 2.82 \times 10^{-5} \text{ \AA}$ ,  $2\theta$  is the angle between the polarisation of the incoming photons and the direction of the outgoing photons. This holds not only for electrons, but for any charged particles with mass (substitute  $q$  for  $e$ ). So if we consider  $Z$  electrons oscillating as one, we have  $Z$  times the mass and  $Z$  times the charge, so the differential cross section per atom with  $Z$  electrons is

$$\left(\frac{d\sigma_{\text{el}}}{d\Omega}\right) = Z^2 r_0^2 (\sin 2\theta)^2. \quad (5.1.2)$$

### Inelastic scattering

Another possibility of scattering is Compton scattering, which can be easily understood: A photon collides with an electron at rest and an amount of energy is transferred onto the electron. Quantitative results for the scattering cross section are far more difficult to derive, and since we will see that Compton scattering is in our case not a big factor, we will make do with looking up the cross section in tables.

**Photoelectric absorption**

The most important effect at energies up to about 100 keV is photoelectric absorption. A photon is absorbed by an atom and its energy is transferred to an electron, which is expelled from the atom. If the ejected electron was situated on an inner shell, the remaining hole will eventually be filled again, either by an electron from an outer shell or by a free electron, in either situation there will be a characteristic amount of energy released, mostly in the form of another photon. The emitted radiation is called fluorescence. Since the electrons in the atom are situated in distinct shells that correspond to distinct energies, the energy dependence of the cross section has discontinuities corresponding to the characteristic energies, because photons with insufficient energy can only interact with electrons in higher shells. If one increases the photon energy by a tiny amount, new interaction possibilities are suddenly given, so the absorption cross section gets suddenly larger. These discontinuities are called edges, labelled as the shells are, that is starting at K and upwards. Especially the K-shell has drastic effects (absorption and fluorescence), the difference in cross section can be one order of magnitude, the influence of outer shells is not so big. Overall, the absorption cross section for a single atom is fairly proportional to  $Z^4$  and  $E^{-3}$ ,  $Z$  the atomic number and  $E$  the photon energy, where the proportionality constant depends only on the accessible shells, not on the element.

**5.2 Comparing samples**

Now back to our problem: only elastic scattering can show interference effects, since interference depends on coherence, and inelastically scattered photons have a different (random) wavelength, so one cannot expect coherence. The same holds with fluorescence, there the photons are emitted randomly and so they have a random phase. So the latter effects give non-correlated background counts, as we have seen, we have to avoid them best possibly. As it turns out, only low- $Z$  elements have Compton scattering cross sections in the order of the elastic scattering cross section, at copper ( $Z = 29$ ) for example the difference is already one order of magnitude. Now to fluorescence: Since the absorption cross section is approximately proportional to  $E^{-3}$  (so the attenuation length goes with  $E^3$ ), there is no problem if there are edges at 2 keV when measuring at 8 keV, because the fluorescence photons then are already attenuated in the sample or at the beryllium windows. But iron, for example, has its K-edge at 7.1 keV, so measuring at 8 keV will give lots of fluorescence. Using SHAPE [SHAPE], an estimate for  $\text{Fe}_{65}\text{Al}_{35}$  at 8 keV was obtained, giving a ratio of elastic scattering to total scattering of 0.01, which is clearly not feasible.

As already pointed out in 2.1, the measured intensity is proportional to the square of the Fourier transform of the charge density, so unless we measure in a Bragg peak, only the non-periodical fluctuations of the charge density contribute to the result, i.e. solute atoms or vacancies. Also we may not forget that (5.1.2) only holds in forward direction because the electrons are not centred in the nucleus. This effect is accounted for by the so-called form factor, which must not be neglected for scattering angles substantially

larger than  $0^\circ$ , consequently. For  $\Delta q$ -values large enough for measuring single atom diffusion, (5.1.2) has to be modified with a factor of about 0.85 for  $2\theta = 15^\circ$ , the relevant data are taken from [Hubbell79]. These data are calculated for isolated atoms, in condensed matter there will be deviations, which are not considered here.

Our aim must be to devise samples with as many inhomogeneities as possible but still not ordered, as large charge fluctuations as possible (that is  $Z$ -differences between constituents) and an absorption cross section as small as possible. As the mass attenuation coefficient  $\frac{\mu}{\rho}$  is readily found tabulated, we have by  $\mu\Delta x = \frac{\sigma_{\text{abs}}nA\Delta x}{A} = \sigma_{\text{abs}}n\Delta x$ , where  $n$  is the number of atoms per volume and  $A$  the irradiated area, the result  $\sigma_{\text{abs}} = \frac{\mu}{\rho}w$ , where  $w$  is the atom weight. The relevant data for a few elements are presented in the following table, data taken from [XRIWM].

element	$Z$	$\sigma_{\text{abs}}$ at 8.0 keV in barns ( $= 10^{-28}m^2$ )
Mg	12	1640
Al	13	2250
Fe	26	28300
Co	27	31800
Cu	29	5540
Ga	31	7290
Ag	47	38800
Au	79	67800

Table 5.1: total cross sections for selected elements

The values of  $\sigma_{\text{abs}}$  obey approximately the  $Z^4$  dependence, the drop at copper is caused by the fact that the K-level is no longer accessible, at gold even the L-level is not accessible. Iron has its K-level at 7.1 keV, cobalt at 7.7 keV, so one has to expect very much fluorescence. The above considered 8.0 keV are a very common value at synchrotrons, in fact most undulators are designed to perform optimally at this value, nevertheless the photon energy is tunable, at [TRO] the range lies between 7 keV and 13 keV, but especially at higher energy the number of photons available drops.

The effect yet to consider is finite longitudinal coherence. As we have seen in 4.2, big values of  $2\theta$  diminish the contrast, but for observing the elementary diffusion step, rather big angles are needed, small angles only yield the macroscopic diffusion constant in the so-called hydrodynamical limit. Just as an example for a possible jump mechanism, figure 5.1 illustrates the expected observed correlation times for nearest-neighbour-jumps on an fcc-lattice with lattice constant  $3.61 \text{ \AA}$  (this is the correct value for copper at room temperature) and 8.9 keV photons along the main directions as a function of  $2\theta$ . As lattice constants generally do not differ substantially, this is representative for all systems mentioned below. We see that the anisotropy is very high for high values of  $2\theta$ , decreasing with decreasing scattering angles. At  $2\theta = 15^\circ$  the ratio of the  $\Gamma$  values drops to 1.15, which appears to be the limit for the anisotropies to be significantly detectable. In figure 5.2 the longitudinal contrast factors due to (4.2.2) for  $L = 3 \mu\text{m}$ , 8.9 keV photons and  $\frac{\Delta E}{E} = 1.428 \times 10^{-4}$  are given for scattering angles of  $15^\circ$ ,  $20^\circ$  and  $25^\circ$  as a function of the sample thickness  $W$ . Obviously the influence of

## 5 Optimising the sample

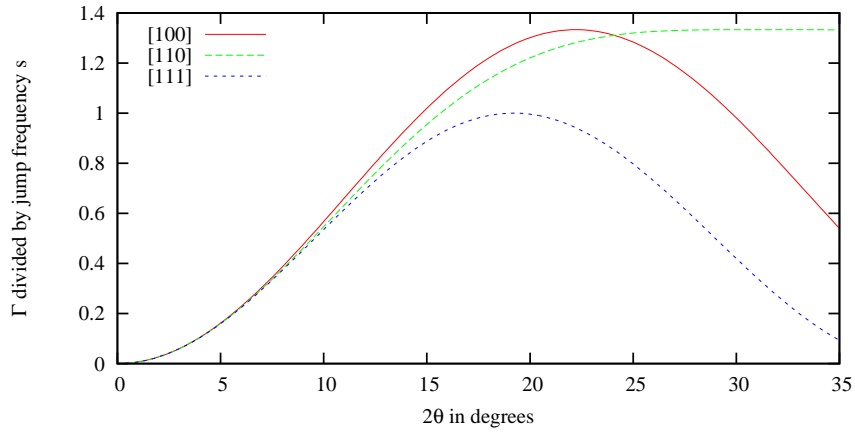


Figure 5.1: angular dependence of  $\Gamma$  along main crystallographic directions in fcc-lattice

the thickness is not so important, once one has set the scattering angle. Also it looks like one can use bigger scattering angles in order to observe more distinct anisotropy with still reasonable contrasts.

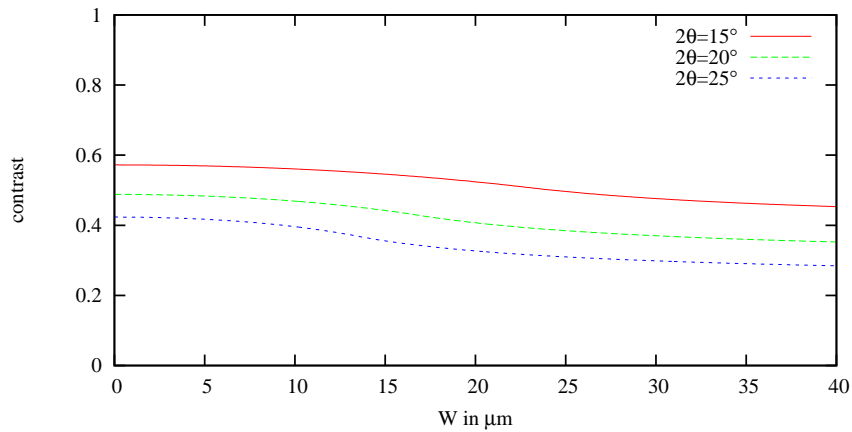


Figure 5.2: dependence on sample thickness  $W$

If we have the attenuation length (which is in the following computed by linear interpolation of the respective densities), the absorption cross section and the differential elastic scattering cross section times pixel solid angle, we can compute the ratio of scattered photons to incident photons as  $\frac{W}{\mu} \frac{\sigma_{\text{el}}}{\sigma_{\text{abs}}} e^{-\frac{W}{\mu}}$ , which is maximised for  $W = \mu$ . The solid angle of one pixel is  $4 \times 10^{-10} \text{ rad}^2$  (with a pixel size of  $(20 \mu\text{m})^2$  and a detector-sample-distance of about 1 meter), the detector efficiency at 8.0 keV is approximately 50%, rising at lower energies, and we have an incident beam of  $1.7 \times 10^{10}$  photons per second. So now all preliminary work is done and we will compare possible samples, with first consideration to 8.0 keV photons and  $2\theta = 15^\circ$  and subsequent discussion

## 5.2 Comparing samples

of possible improvements,  $\Delta Z_{\text{eff}}$  takes the finite extension of the charge density of one atom into account.

sample composition	$(\Delta Z_{\text{eff}})^2$ at 8.0 keV	mean $\sigma_{\text{abs}}$ for 8.0 keV in barns
Co <sub>60</sub> Ga <sub>40</sub>	15.58	22000

The reason for considering this system is that in our group measurements were already performed on it [Stadler06a], so the sample and first-hand experience is available. Cobalt has its K-edge at 7.7 keV, so it would be really unwise to measure at 8 keV. Therefore we go just below the K-edge and have 23  $\mu\text{m}$  attenuation length. The averaged absorption cross section is 4340 barn per atom, the elastic differential cross section times pixel solid angle (also taking into account above mentioned factor for non-forward direction) is  $4.96 \times 10^{-11}$  barn per atom, that means the ratio of elastic cross section and absorption cross section is  $1.14 \times 10^{-14}$ , which yields a count rate of  $3.65 \times 10^{-5}$  photons per second and pixel (detector efficiency taken into account), so we would have to wait seven hours to detect one photon, which obviously is not feasible.

sample composition	$(\Delta Z_{\text{eff}})^2$ at 8.0 keV	mean $\sigma_{\text{abs}}$ for 8.0 keV in barns
Fe <sub>65</sub> Al <sub>35</sub>	159.0	19200

This system is very well-known, since it contains iron and is therefore predestined for Mößbauer measurements. Again one would have nothing but fluorescence for 8 keV, so we go to 7.1 keV, there we have an attenuation length of about 30  $\mu\text{m}$  and an averaged absorption cross section of 4180 barn per atom. The elastic differential cross section times pixel solid angle gives  $7.69 \times 10^{-10}$  barn per atom, so the ratio of elastic cross section and absorption cross section is  $1.84 \times 10^{-13}$ , and so we have  $6.21 \times 10^{-4}$  counts per second and pixel with  $W = 30 \mu\text{m}$ , which is 2.2 counts per hour. This is not much, still, also we now have a very bad contrast.

sample composition	$(\Delta Z_{\text{eff}})^2$ at 8.0 keV	mean $\sigma_{\text{abs}}$ for 8.0 keV in barns
Ag <sub>60</sub> Mg <sub>40</sub>	1154	23900

This is a rather exotic system, it was considered because of the high relative charge difference. This time measuring at 8.0 keV seems to be appropriate, probably a little more would be better, since silver has its L-edges at 3.8 keV. Silver is a rather heavy element, and so we have an attenuation length of about 7.6  $\mu\text{m}$ . The elastic differential cross section times pixel solid angle is  $3.67 \times 10^{-9}$  barn per atom, the ratio is  $2.11 \times 10^{-13}$ , if we assume a sample thickness of 7  $\mu\text{m}$  we have a count rate of  $6.6 \times 10^{-4}$  counts per second and pixel, which is 2.3 counts per hour, a little more than above, now also the contrast will be better, since the sample thickness is much smaller.

sample composition	$(\Delta Z_{\text{eff}})^2$ at 8.0 keV	mean $\sigma_{\text{abs}}$ for 8.0 keV in barns
Cu <sub>90</sub> Au <sub>10</sub>	2360	11800

This is the simplest system so far, since here the Au-atoms are randomly distributed (except maybe for some kind of near order), and there are not two sublattices which give rise to two correlation times. The choice of 8.9 keV is optimal for this system, since this is just below the K-edge of copper. The attenuation length is then given by approximately 14.5  $\mu\text{m}$ , the averaged elastic differential cross section per atom times

## 5 Optimising the sample

pixel solid angle is  $7.41 \times 10^{-9}$  barn, the ratio of elastic cross section and absorption cross section is  $8.68 \times 10^{-13}$ , for a sample thickness of  $14 \mu\text{m}$  and a detector efficiency of 40% we have a count rate of  $2.17 \times 10^{-3}$  per second and pixel, this means about 7.8 counts per hour, which should be measurable.

### 5.3 Proposing an experiment

To demonstrate the feasibility of observing the elementary diffusion step with XPCS, we propose the following experiment: We take the system  $\text{Cu}_{90}\text{Au}_{10}$  at a sample thickness of  $14 \mu\text{m}$ , we choose 8.9 keV photons with the least possible monochromatisation, that is  $\frac{\Delta E}{E} = 1.428 \times 10^{-4}$ . We use vertical focussing to obtain equal vertical and horizontal effective source sizes of approximately 928 mrad each, so we have to use a pinhole of  $3 \times 3 \mu\text{m}^2$  to get a reasonable transversal coherence factor, namely 0.51 with a detector distance of 1 m due to section 4.2. Choosing a scattering angle of  $2\theta = 20^\circ$ , we have a longitudinal coherence factor of 0.45, and since we have chosen the X-ray energy with an eye on the relevant K-edges, we expect no fluorescence (at least in the relevant energy range, low photon energies of the Au-M-edges at 3 keV will be cut off by the beryllium window of the detector or recognised due to the energy resolution of the detector). So we expect an overall contrast of approximately 0.22 with a count rate of 4.3 photons per pixel and hour.

We now assume the maximum measurement time to be 3 hours, for example governed by the stability of the beam, and we assume that unavoidable events that cause the correlation to be lost, e.g. movements of the sample, occur randomly with a mean rate of once per hour. Using the experience gained in chapter 3 we decide on 15 minutes to be a well measurable correlation time, and we expect 20000 pixel to be enough for a SNR of about 10. In a cubic lattice the macroscopic diffusion constant  $D$  is given by  $D = \frac{1}{6}d_{\text{NN}}^2s$  with  $d_{\text{NN}}$  the nearest-neighbour distance and  $s$  the jump frequency, for a correlation time of 900 along [111] we need a jump frequency  $s$  of  $8.54 \times 10^{-4} \text{s}^{-1}$ . So we need values of  $D = 9.51 \times 10^{-24} \text{m}^2\text{s}^{-1}$ , due to [Fujikawa87] this corresponds to a temperature of about 560 K. The problem is that diffusion constants are generally not precisely known, different methods of measurement yield often different diffusion constants. In the considered temperature region a change of just 1 K corresponds to a change in the diffusion coefficient of about 10%, so finding the right temperature is crucial. Assuming that we have set the temperature to yield a correlation time of 900 seconds along [111], we have for the model of nearest-neighbour diffusion (which is most likely the true model) correlation times of 844 seconds along [110] and 689 seconds along [111]. We set the frame exposure time at 50 seconds, so the read-out time (which is typically in the range of a few seconds) is negligible. Based on these assumptions, we now carry out simulations with the expected count rate, the above mentioned correlation losses are also taken into account. The fitted correlation times are presented in table 5.2, the auto-correlation function for the second run of [100] is given in figure 5.3.

Discussing the results of table 5.2, we see that the deviations from the predicted value



## 5.4 Discussion of an already performed experiment

	[100]	[110]	[111]
expected values	900	844	689
simulations	807	746	708
	820	837	622

Table 5.2: simulated correlation times

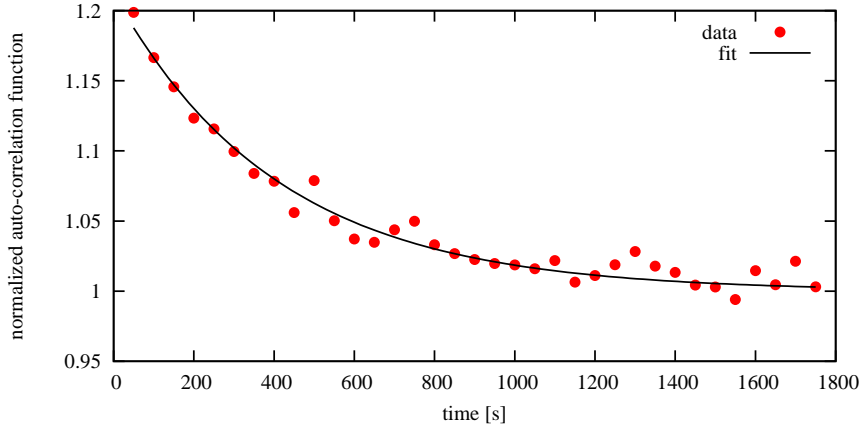


Figure 5.3: fitted auto-correlation from a run along [100]

are considerable, and each time but one the simulated correlation time was shorter than the predicted one. This is easily understood, since we also simulated correlation losses, which make the auto-correlation function fall faster than it would without them. Figure 5.3 shows that a higher count rate or more pixels to be averaged over are no remedy, since the statistical deviations from the fitted line are rather small. In fact, the deviations of the fitted correlation times are heavily correlated with the number of correlations losses in the respective run, but the expected tendency is already discernible. We now have used only 20000 of the 1.7 million available pixels, so one way to get a better SNR would be to use shorter expected correlation times and shorter measurement times, but more pixels. Because of the shorter measurement times, it is possible to do more runs of the same situation, fit each run for itself, and if one run yields a significantly shorter correlation time, one can conclude that a correlation loss has happened and discard that run. Since these phenomena are not predictable, one will have to decide at the beamline by trial and error on the optimal expected correlation times and measurement times, but from the example presented here, one can expect the experiment to be successful.

## 5.4 Discussion of an already performed experiment

Until now we have only spoken of the possibility of measuring atomic diffusion in crystalline solids. In contrast to glass-like matter crystalline solids have the advantage that

## 5 Optimising the sample

there exist a few possible models for diffusion, for example in an B2-ordered alloy, the two main candidates are nearest-neighbour jumps via anti-structure sites opposed to jumps within the sublattice. Once one has experimental data of sufficient quality, it is relatively easy to decide between the two models. On the other hand, in glass-like matter one can only hope to measure the probability distribution of the length of the jumps, and in an alloy it will be extremely difficult (with non-resonant methods) to come up with separate probability distributions for the jump lengths of the respective components. But there is one advantage: Since glasses are not ordered, there are no Bragg peaks, the scattered intensity is comparatively equal for all directions, so the measured diffuse intensity is much higher. This is the reason why in our group it was attempted to measure atomic diffusion in metallic glasses, specifically  $\text{Zr}_{65}\text{Ni}_{10}\text{Cu}_{17.5}\text{Al}_{7.5}$  was used as sample. Metallic glasses are not in equilibrium, because the ordered state is energetically favourable, so one always has to mind not to heat them too much, otherwise crystallisation would occur. For the sample at hand plenty of data were available [Faupel03, Mayer96], and a relevant temperature range of  $100^\circ - 250^\circ\text{C}$  was estimated. In a scan along  $2\theta$  a sharp peak occurred at about  $2\theta = 6^\circ$  which corresponds to distances of about  $15 \text{ \AA}$ , the expected glass peak was at about  $2\theta = 36^\circ$  which corresponds to  $2.5 \text{ \AA}$ . Because of the high scattered intensity, all subsequent measurements were taken at the position of the peak at  $2\theta = 6^\circ$ , without finding an explanation for it. Unfortunately, the measured data shows no utilisable information. Figure 5.4 is the auto-correlation function of 50000 pixels at  $100^\circ\text{C}$ .

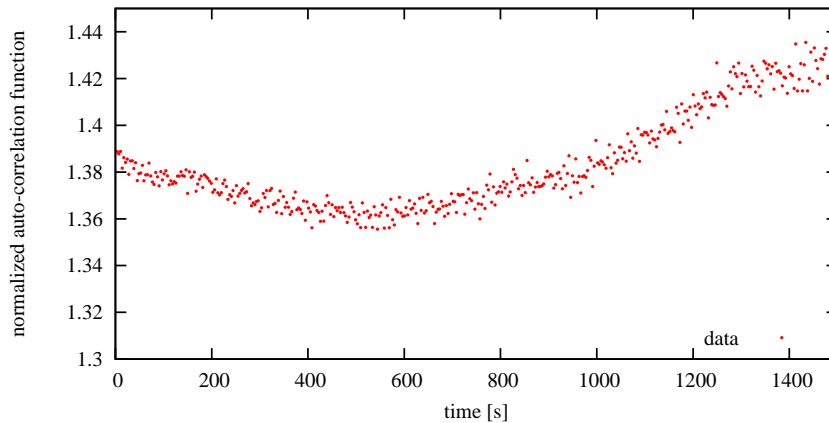


Figure 5.4: normalized experimental auto-correlation function

The mean counts per pixel, integrated over the whole experiment, are about 10, clearly that is enough, since the statistical deviations of the single points is very small. It is tempting to interpret the slope at short times as exponential decay, but in fact this chart is a perfect example of what can go wrong. First of all, the auto-correlation function rises again for longer times. This effect is caused by the instable overall scattered intensity (probably caused by the beam), given in figure 5.5. If one excludes the first 500 frames, the auto-correlation function is more or less a straight

#### 5.4 Discussion of an already performed experiment

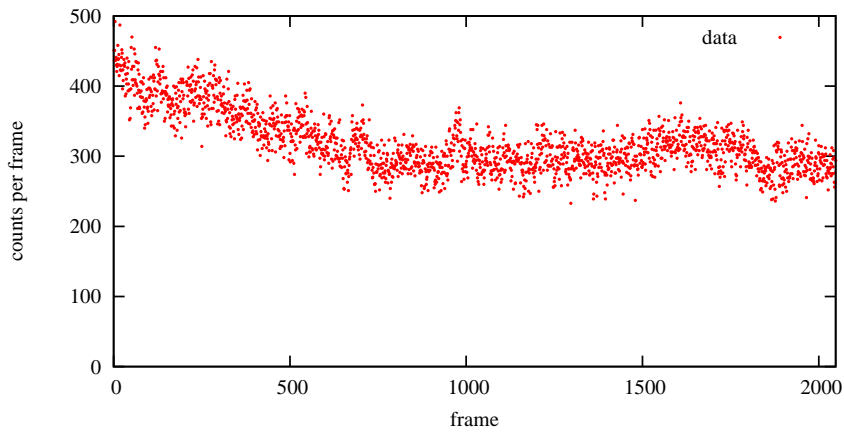


Figure 5.5: intensity fluctuations

horizontal line. The auto-correlation functions for 200°C and 250°C also show no features. A statistical treatment of the distribution of the counts summed over the whole measurement time shows contrasts of 0.0517, 0.0511 and 0.0554 for the three temperatures. That means, it looks like the beam coherence factor was only 0.05, or the total measurement time was 20 correlation times. Since the observed value is independent of the temperature, the latter explanation can be discarded, the former one contradicts the beamline-settings. Perhaps the most simple explanation is the true one: the peak at  $2\theta = 6^\circ$  was not caused by the sample, but rather by the optics, and most of the counts were just uncorrelated background.

## 5 *Optimising the sample*

## 6 Conclusion

In the course of this thesis it was shown that X-ray photon correlation spectroscopy is feasible at count rates of just 3 counts per pixel and measurement time under the condition of stable beam and sample. It was pointed out that by optimising the beam-line setup, it should be possible to measure atomic diffusion even with today's X-ray sources in selected samples, one example being  $\text{Cu}_{90}\text{Au}_{10}$ . Due to [XFEL], in a few years sources with an average brilliance of  $10^4$  times more than today will become available. Due to the high expected count rate, it will be possible to choose the correlation times very short compared to the values considered here, so the problems encountered here (that is correlation losses during the measurement time) will vanish. In section 5.2 it was shown that even samples that seem extremely unfit for XPCS only yield count rates of about  $10^2$  times lower than the best ones, so it seems that XPCS diffusion studies on atomic level will be possible with X-ray free electron lasers on a wide range of samples.

## 6 Conclusion

# Notation

$a, b, d, e$	defined on page 7
$A$	amplitude
$A$	contrast (zero-shift-time limit of auto-correlation function)
$A_j$	contribution to amplitude of $j$ scattering centre
$B$	brilliance
$c$	mean background radiation in terms of $I_0$
$C$	normalisation factor in various contexts
$C_{i,j}$	covariance of contributions of $i$ th and $j$ scatterer to amplitude
$C_{i,j}$	covariance of photon counts in frames $i$ and $j$
$C_{\Delta k, \Delta l}$	covariance of two points of the auto-correlation function
$d_{\text{NN}}$	nearest-neighbour distance
$D$	diffusion constant
$f$	range over which the auto-correlation function is fitted in times of $\tau$
$f_i$	atomic form factors
$g_2(t)$	intensity auto-correlation function
$g'(t)$	measured auto-correlation function
$H$	number of speckles per pixel
$I$	intensity (number of photons per time)
$I_k$	counts in frame $k$ (in one distinct pixel)
$\bar{I}$	instantaneous intensity
$I_0$	mean intensity
$K$	number of frames considered
$L$	number of atoms in the matrix
$L_x, L_z$	horizontal and vertical dimension of pinhole (assumed rectangular)
$M$	number of pixels averaged over
$N$	number of scattering centres
$N_j$	number of scattering centres jumping $j$ times
$P(\varphi)$	probability density of contribution of single scattering centre to amplitude
$P(\varphi_1, \varphi_2)$	two-scatterer probability distribution
$P_A(x + iy)$	probability density of amplitude
$p$	expected counts per pixel over the whole experimental duration
$p_j$	probability of $s_j$
$q_0$	length of wave vector of incident wave
$\Delta q$	length of difference of incident and outgoing wave vectors

## 6 Conclusion

$r_j$	position of $j$ th scattering centre
$r_0$	Thomson's electron radius
$R_j$	$j$ th lattice point
$s$	jump frequency
$s_j$	atomic jump vectors
$s^j(\varphi)$	probability density of amplitude after jumping $j$ times
$t$	time (in all possible contexts)
$T$	experimental duration
$T_f$	exposure time per frame
$V$	illuminated (scattering) volume
$V_{\Delta k}$	variance of auto-correlation function in $\Delta k$
$Z$	atomic number
$\gamma$	correlation exponent for long-term correlations
$\Gamma$	inverse of correlation time
$\delta$	optical path-length difference
$\varepsilon$	number of possible jump vectors
$\theta$	so-called scattering angle (half of angle between incident and outgoing wave)
$\vartheta_x, \vartheta_z$	horizontal and vertical effective angular source size
$\Theta_x, \Theta_z$	horizontal and vertical effective coherence length
$\lambda$	(mean) wavelength of incident photons
$\Lambda$	longitudinal coherence length
$\sigma_r, \sigma_i$	standard deviation of amplitude in real and imaginary direction
$\sigma_{\text{rel}}$	relative standard deviation of auto-correlation function
$\sigma_x, \sigma_z$	horizontal and vertical source size
$\sigma_{\text{el}}$	elastic (coherent) scattering cross section
$\sigma_{\text{abs}}$	absorption cross section
$\tau$	correlation time
$\varphi_j$	angle of contribution to amplitude of scattering centre $j$
$\phi$	incident flux
$\omega_x, \omega_z$	horizontal and vertical angular pixel size



# Bibliography

- [Als-Nielsen01] J. Als-Nielsen, D. McMorrow, “Elements of Modern X-Ray Physics”, John Wiley & Sons Ltd, Chichester (2001).
- [Ashcroft76] N. W. Ashcroft, N. D. Mermin, “Solid State Physics”, Saunders College Publishing, United States (1976).
- [Falus06] P. Falus, L.B. Lurio, S.G.J. Mochrie, “Optimizing the signal-to-noise ration for X-ray photon correlation spectroscopy”, *J. Synchrotron Rad.* **13**, 253 (2006).
- [Faupel03] F. Faupel, W. Frank, M.-P. Macht, H. Mehrer, V. Naundorf, K. Rätzke, H. Schober, S. Sharma, H. Teichler, “Diffusion in metallic glasses and supercooled melts”, *Rev. Mod. Phys.* **75**, 237 (2003).
- [Fujikawa87] S. Fujikawa, M. Werner, H. Mehrer, A. Seeger, “Diffusion of gold in copper over a wide range of temperature”, *Mat. Sci. Forum* **15-18**, 431 (1987).
- [Goodman85] J. W. Goodman, “Statistical Optics”, John Wiley & Sons, Inc., New York (1985).
- [Hubbell79] J.H. Hubbell, I. Øverbø, “Relativistic Atomic Form Factors and Photon Coherent Scattering Cross Sections”, *J. Phys. Chem. Ref. Data* **8**, 1, 63 (1979).
- [Jakeman73] E. Jakeman, “Photon Correlation and Light Beating Spectroscopy”, eds. H.Z. Cummins, E.R. Pike, Plenum, New York (1973).
- [Kaisermayr01a] M. Kaisermayr, J. Combet, H. Ipsen, H. Schicketanz, B. Sepiol, G. Vogl, “Determination of the elementary jump of Co in CoGa by quasielastic neutron scattering”, *Phys. Rev. B* **63**, 054303 (2001).
- [Kaisermayr01b] M. Kaisermayr, C. Pappas, B. Sepiol, G. Vogl, “Probing Jump Diffusion in Crystalline Solids with Neutron Spin-Echo Spectroscopy”, *Phys. Rev. Lett.* **87**, 175901 (2001).
- [Kandelhardt01] J. W. Kandelhardt, E. Koscielny-Bunde, H. H. A. Rego, S. Havlin, A. Bunde, “Detecting long-range correlations with detrended fluctuation analysis”, *Physica A* **295**, 441 (2001).
- [Mayer96] A. Meyer, J. Wuttke, W. Petry, A. Peker, R. Bormann, G. Coddens, L. Kranich, O. G. Randl, H. Schober, “Harmonic behavior of metallic glasses up to the metastable melt”, *Phys. Rev. B* **53**, 12107 (1996).

## Bibliography

- [Mochrie00] D. Lumma, L.B. Lurio, S.G.J. Mochrie, M. Sutton, “Area detector based photon correlation in the regime of short data batches: Data reduction for dynamic x-ray scattering”, *Rev. Sci. Instrum.* **71**, 3274 (2000).
- [Pfau06a] B. Pfau, “Kombination von Photonenkorrelationsspektroskopie und Fluktuationsanalyse zur Untersuchung von Diffusionsdynamik”, diploma thesis, Fakultät Mathematik und Naturwissenschaften, TU Dresden (2006).
- [Pfau06b] B. Pfau, L.-M. Stadler, B. Sepiol, R. Weinkamer, J. W. Kantelhardt, F. Zontone, G. Vogl, “Coarsening dynamics in elastically anisotropic alloys”, *Phys. Rev. B* **73**, 180101(R) (2006).
- [Sandy99] A. R. Sandy, L. B. Lurio, S. G. J. Mochrie, A. Malik, G. B. Stephenson, J. F. Pelletier, M. Sutton, “Design and characterization of an undulator beamline optimized for small-angle coherent X-ray scattering at the Advanced Photon Source”, *J. Synchrotron Rad.* **6**, 1174 (1999).
- [Sepiol93] B. Sepiol, G. Vogl, “Atomistic Determination of Diffusion Mechanism on an Ordered Lattice”, *Phys. Rev. Lett.* **71**, 731 (1993).
- [Sepiol96] B. Sepiol, A. Meyer, G. Vogl, R. Ruffer, A. I. Chumakov, A. Q. R. Baron, “Time Domain Study of  $^{57}\text{Fe}$  Diffusion using Nuclear Forward Scattering of Synchrotron Radiation”, *Phys. Rev. Lett.* **76**, 3220 (1996).
- [SHAPE] URL <http://shape.ing.unibo.it/html/shape.html>
- [Stadler03] L.-M. Stadler, B. Sepiol, R. Weinkamer, M. Hartmann, P. Fratzl, J. W. Kantelhardt, F. Zontone, G. Grübel, G. Vogl, “Long-term correlations distinguish coarsening mechanisms in alloys”, *Phys. Rev. B* **68**, 180101(R) (2003).
- [Stadler06a] L.-M. Stadler, “Dynamics investigations in solids with coherent X-rays”, Ph.D. thesis, Fakultät für Physik, Universität Wien (2006).
- [Stadler06b] L.M.Stadler, B. Sepiol, B. Pfau, J.W. Kantelhardt, R. Weinkamer, G. Vogl, “Detrended Fluctuation Analysis in X-ray Photon Correlation Spectroscopy for determining coarsening dynamics in alloys”, *Phys. Rev. E* **74**, 041107 (2006).
- [TRO] URL <http://www.esrf.eu/UsersAndScience/Experiments/SCMatter/ID10A/>
- [Vogl98] G. Vogl, R. Feldwisch, “Diffusion in Condensed Matter”, eds. J. Kärger, P. Heitjans, R. Haberlandt, Vieweg, Braunschweig/Wiesbaden (1998).
- [XFEL] URL [http://tesla.desy.de/new\\_pages/TDR\\_CD/PartV/fel.html](http://tesla.desy.de/new_pages/TDR_CD/PartV/fel.html), <http://www-ssrl.slac.stanford.edu/lcls/>
- [XRIWM] URL [http://www-cxro.lbl.gov/optical\\_constants/](http://www-cxro.lbl.gov/optical_constants/)

# Curriculum vitae

Name: Michael Leitner  
Date of birth: October 13th, 1982  
Place of birth: Mistelbach, Austria  
Parents: Maria Leitner, nee Krschka  
Werner Leitner

1989–1993: Volksschule Neudorf  
1993–2001: Bundesgymnasium Laa

2001–2002: Military service

2002–: Diploma studies in mathematics at the University of Vienna  
2003–2007: Diploma studies in physics at the University of Vienna